ELSEVIER

Journal of Alloys and Compounds xxx (2007) xxx–xxx

Journal of ALLOYS AND COMPOUNDS

www.elsevier.com/locate/jallcom

Dielectric and ferroelectric properties of fine grains $Pb(In_{1/2}Nb_{1/2})O_3$–$PbTiO_3$ ceramics

Supattra Wongsaenmai [a], Xiaoli Tan [b], Supon Ananta [a], Rattikorn Yimnirun [a,*]

[a] *Department of Physics, Faculty of Science, Chiang Mai University, Chiang Mai 50200, Thailand*
[b] *Department of Materials Science and Engineering, Iowa State University, Ames, IA 50011, USA*

Received 3 October 2006; accepted 10 December 2006

Abstract

The dielectric and ferroelectric properties of $(1-x)Pb(In_{1/2}Nb_{1/2})O_3$–$xPbTiO_3$ (when $x = 0.1$, 0.2, 0.3, 0.4, and 0.5) ceramics prepared by an oxide-mixing method via a vibro-milling technique were investigated. Fine grains ceramics were achieved with average grain size of 1–2 μm, indicating advantage of the vibro-milling technique used. While PIN ceramic exhibited relaxor behavior, the dielectric properties of PIN–PT ceramics showed a mixed relaxor and normal ferroelectric behavior, with more normal ferroelectric behavior observed with increasing PT content. In addition, the ferroelectric properties of the ceramics in PIN–PT system changed from the relaxor ferroelectric behavior in PIN ceramic to the normal ferroelectric behavior in PIN–PT ceramics. These results clearly show the significance of the added PT in reducing the relaxor ferroelectric behavior in PIN ceramic. Finally, the existence of the MPB composition between $x = 0.3$ and 0.4 has been confirmed from the XRD analysis, and dielectric and ferroelectric properties measurements.

Keywords: Dielectric properties; Ferroelectric properties; Mixed-oxide; PIN–PT

1. Introduction

Lead-based perovskite-type solid solutions consisting of the ferroelectric and relaxor materials have attracted a growing fundamental and practical interest because of their excellent dielectric, piezoelectric and electrostrictive properties which are useful in actuating and sensing applications [1–3]. Among the lead-based complex perovskites, lead magnesium niobate–lead titanate ($(1-x)Pb(Mg_{1/3}Nb_{2/3})O_3$–$xPbTiO_3$ or PMN-PT) and lead zinc niobate–lead titanate ($(1-x)Pb(Zn_{1/3}Nb_{2/3})O_3$–$xPbTiO_3$ or PZN-PT) have attracted much attention due to their superior electrical properties [4–7]. However, the major disadvantage of the two ceramic systems is relatively low Curie temperatures (T_C) of the morphotropic phase boundary (MPB) compositions, i.e. lower than 200 °C for the two systems [5–8]. This low T_C comes with the expenses of more temperature dependent properties and less polarization stability, which in turn restrict the operating temperature range to less than 100 °C [7,8]. Interestingly, the MPB composition of the lead indium niobate–lead titanate ($(1-x)Pb(In_{1/2}Nb_{1/2})O_3$–$xPbTiO_3$ or PIN–PT) solid solution system has been reported to possess T_C higher than 250 °C [8–13], and therefore potential for high temperature applications. Many previous studies have focused on the processing and properties of PIN–PT single crystals, particularly the MPB composition [9,12,14,15], while the information on PIN–PT ceramics is still limited [8,10,13]. In addition, most of the PIN–PT ceramics studied were prepared by the mixed-oxide method with a conventional ball-milling technique, which resulted in coarse grains ceramics [11,13], even though it is well known that fine grains ceramics usually show superior electrical properties [16,17]. Recently, a vibro-milling technique has been employed to produce nano-sized powders which can be used to fabricate ceramics with fine grain microstructure [18–20]. Therefore, as an extension to the research on the PIN–PT ceramics, the overall purpose of this study was to systematically determine the dielectric and ferroelectric properties of ceramics in the $(1-x)Pb(In_{1/2}Nb_{1/2})O_3$–$xPbTiO_3$ (when $x = 0.0$, 0.1, 0.2, 0.3, 0.4, and 0.5) system prepared by the mixed-oxide method via the vibro-milling technique. The vibro-milling technique

* Corresponding author. Tel.: +66 53 943 367; fax: +66 53 943 445.
E-mail addresses: rattikor@chiangmai.ac.th, rattikornyimnirun@yahoo.com (R. Yimnirun).

0925-8388/$ – see front matter © 2006 Elsevier B.V. All rights reserved.
doi:10.1016/j.jallcom.2006.12.053

was employed to explore the potential in obtaining fine grains ceramics, which would in turn lead to superior electrical properties.

2. Experimental

The $Pb(In_{1/2}Nb_{1/2})O_3$–$PbTiO_3$ ceramics used in this study were prepared from $Pb(In_{1/2}Nb_{1/2})O_3$ and $PbTiO_3$ starting powders obtained via the vibro-milling technique. In this technique, a vibratory laboratory mill (McCrone Micronizing Mill) was employed. A total of 48 polycrystalline corundum milling media with a powder weight of 20 g was kept constant in each batch. The milling operation was carried out in isopropanal inert to the polypropylene jar [18–20]. Initially, pure-phase PIN powders were obtained via a well-known wolframite method [21,22], while PT powders were prepared by a mixed-oxide method [23]. With the wolframite method, the single-phase indium niobate ($InNbO_4$) powders were first prepared by mixing starting indium oxide (In_2O_3) and niobium oxide (Nb_2O_5) (Aldrich, 99.9% purity) powders by employing the vibro-milling technique for 0.5 h and then calcining the mixed powders at 900 °C for 4 h with heating/cooling rates of 30 °C/min [24]. This yielded a so-called wolframite ($InNbO_4$) powder. The wolframite precursor powders were subsequently vibro-milled with lead oxide (PbO) (Fluka, 99% purity) for 0.5 h. The mixed powders were calcined at 1100 °C for 2 h with heating/cooling rates of 10 °C/min to form a single-phase PIN [25]. It should, however, be noted that to obtain the pure-phase PIN powders 2 mol% excess of In_2O_3 and PbO had to be added to compensate the loss during calcination [25]. With a more conventional oxide-mixing route, PT powders were prepared from PbO and titanium oxide (TiO_2) (Riedel-de Haën, 99% purity) starting powders. These powders were vibro-milled for 0.5 h and later calcined at 600 °C for 2 h with heating/cooling rates of 5 °C/min [23]. The $(1-x)Pb(In_{1/2}Nb_{1/2})O_3$–$xPbTiO_3$ (when $x = 0.0, 0.1, 0.2, 0.3, 0.4$, and 0.5) ceramics were then prepared from the PIN and PT powders by the same mixed-oxide method. The PIN and PT powders were weighed in the required stoichiometric ratio and vibro-milled for 0.5. The thoroughly mixed powders were then pressed hydraulically to form disc-shaped pellets 10 mm in diameter and 2 mm thick, with 3 wt.% polyvinyl alcohol as a binder. The pellets were placed on the alumina powder-bed inside alumina crucible and surrounded with atmosphere powders of the same composition. Finally, the pellets were sintered at 1175 °C (1050 °C for PIN) for 2 h with heating/cooling rates of 10 °C/min.

The densities of the sintered ceramics were measured by Archimedes method. The phase formations of the sintered specimens were studied by an X-ray diffractometer (XRD; Siemen-D500 diffractometer). The microstructure analyses were undertaken by a scanning electron microscopy (SEM: JEOL Model JSM 840A). Grain size was determined from SEM micrographs by a linear intercept method. The dielectric properties were evaluated with a computer-controlled dielectric measurement system consisted of a precision LCR-meter (Hewlett Packard, model 4284A), a temperature chamber (Delta Design, model 9023), and a sample holder (Norwegian Electroceramics) capable of high temperature measurement. The room temperature ferroelectric polarization versus electric field (*P–E*) measurements was made using a standardized ferroelectric test system (RT-66A, Radiant Technologies) with an applied field of 30–60 kV/cm.

3. Results and discussion

The XRD patterns of $(1-x)$PIN–xPT ceramics with various x values are shown in Fig. 1(a). It can be seen that a complete crystalline solution of perovskite structure is formed throughout the composition range without the presence of pyrochlore or unwanted phases. From the patterns, PIN ceramic is identified as a single-phase material with a perovskite structure having cubic symmetry which could be matched with JCPDS file no. 87-0304. The XRD patterns of the PIN–PT compositions show a combination between PIN and PT patterns, showing a perovskite structure having the symmetry varying between pseudo-cubic and tetragonal types. For better comparison, the

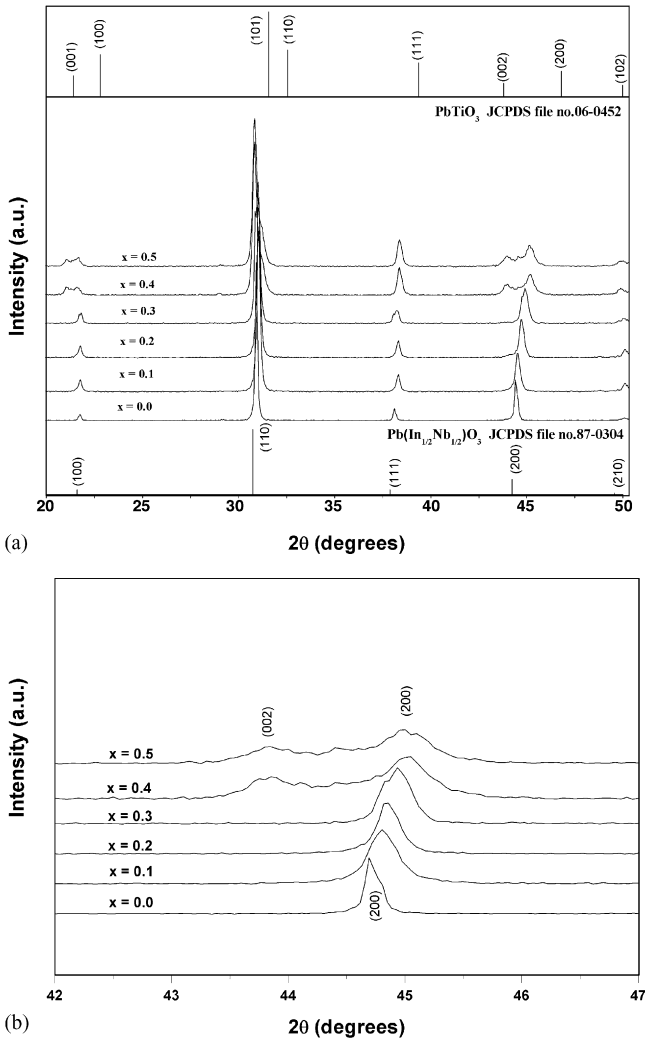

Fig. 1. (a) XRD patterns of $(1-x)$PIN–xPT ceramics and (b) selected region of the diffraction patterns.

JCPDS file no. 06-0452 for PT with a tetragonal structural symmetry is also displayed in Fig. 1(a). More interestingly, the composition with $x = 0.3$ began to exhibit broadening of peaks at $2\theta \approx 21.5°$, 30.5°, and 44.5° for (1 0 0)/(0 0 1), (1 1 0)/(1 0 1), and (2 0 0)/(0 0 2), respectively. Fig. 1(b) shows the broadened peaks at $2\theta \sim 44.5$–45°, indicating the structural transformation from the pseudo-cubic phase to the tetragonal phase, characterized by (2 0 0)/(0 0 2) peaks. This observation is obviously associated with the composition with coexistence of two symmetries, which in this case are tetragonal and pseudo-cubic phases. To a first approximation, it could be said that the composition between $x = 0.3$ and 0.4 is close to the morphotropic phase boundary (MPB) of the $Pb(In_{1/2}Nb_{1/2})O_3$–$PbTiO_3$ system, where the structure of the PIN–PT compositions is gradually changing from pseudo-cubic to tetragonal. Earlier studies have reported the MPB composition for PIN–PT system at $x \sim 0.37$ [9–12]. Electrical data described later further support this observation.

SEM micrographs in Fig. 2 reveal fine grains microstructure in all PIN–PT ceramics with little variation of the average grain

Please cite this article in press as: S. Wongsaenmai et al., J. Alloys Compd. (2007), doi:10.1016/j.jallcom.2006.12.053

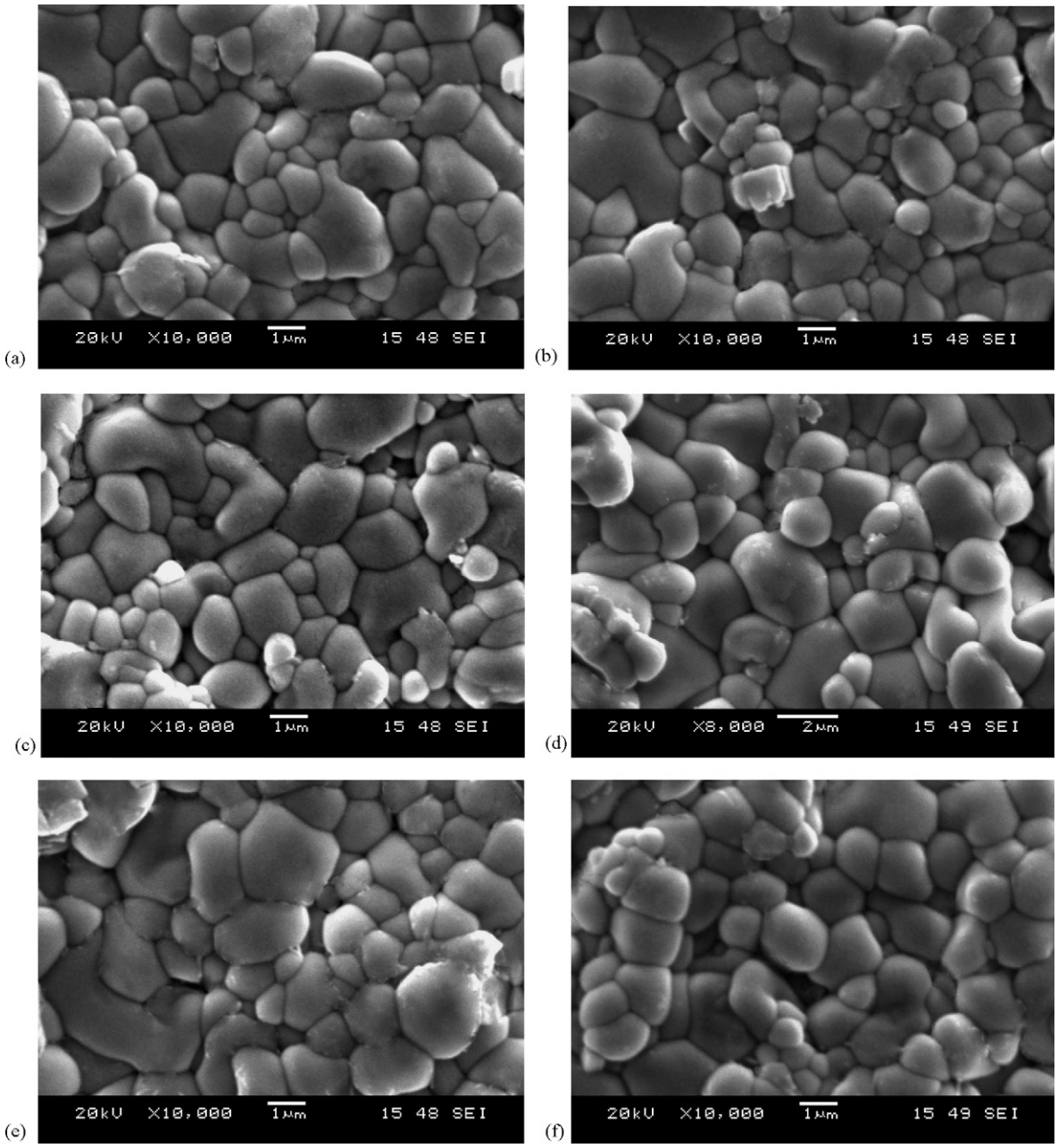

Fig. 2. SEM micrographs of $(1-x)$PIN–xPT with various compositions: (a) $x=0.0$, (b) $x=0.1$, (c) $x=0.2$, (d) $x=0.3$, (e) $x=0.4$, and (f) $x=0.5$.

size between 1 and 2 μm. The average grain size, as well as the density, does not vary significantly with the ceramic compositions, as listed in Table 1. However, it should be noticed that the microstructure of all the compositions also represents two distinct grain sizes, i.e. large grains (∼2 μm) and submicron grains. Earlier study on PIN–PT ceramics prepared with the conventional ball-milling method has also reported bimodal grain sizes but with large grains over 10 μm and fine grains about 1–2 μm [10]. Clearly, this shows the advantage of the vibro-milling technique in producing fine grains PIN–PT ceramics.

The dielectric properties, e.g. dielectric constant (ε_r) and $\tan\delta$, are measured as functions of both temperature and frequency, as shown in Fig. 3(a)–(f). As listed in Table 1 and plotted separately in Fig. 4, the maximum dielectric constant increases steadily with increasing PT content up to 30 mol% (ε_r increases from 4310 in PIN to 16028 in 0.7PIN–0.3PT). Then a drop in the dielectric constant is observed with further increase in PT content to 40 mol%. This supports the XRD observation that the MPB composition should lie between compositions $x=0.3$ and 0.4. It should also be noted that a rise in the dielectric constant with more PT content (50 mol%) is possibly caused by large thermal conduction at high temperature [26]. Furthermore, as listed in Table 1, since the transition temperature of PT is very high (490 °C) [27], it is expected to observe that the transition temperature increases with increasing amount of PT in the PIN–PT system. This is clearly evident in Fig. 4. Again, it should also be noted here that, as shown in Fig. 3, the dielectric properties of most compositions increase significantly at high temperature

Please cite this article in press as: S. Wongsaenmai et al., J. Alloys Compd. (2007), doi:10.1016/j.jallcom.2006.12.053

Table 1
Physical features and dielectric properties of $(1-x)$PIN–xPT ceramics (measured at 1 kHz)

x	Density (g/cm^3)	Grain size (μm)	T_{max} (°C)	ε_r at		$\Delta T = T_{m,100\,kHz} - T_{m,100\,Hz}$ (°C)	Diffusivity (γ)
				T_{max}	25 °C		
0.0	7.83	1.22 ± 0.08	71	4310	3345	26.2	1.89
0.1	7.51	1.29 ± 0.10	175	7120	2336	8.0	1.83
0.2	7.95	1.41 ± 0.12	210	10,733	1659	5.4	1.75
0.3	8.09	1.84 ± 0.16	267	16,028	1056	1.6	1.70
0.4	7.98	1.51 ± 0.16	327	11,867	1291	1.0	1.65
0.5	7.95	1.33 ± 0.10	375	15,038	573	0.4	1.62

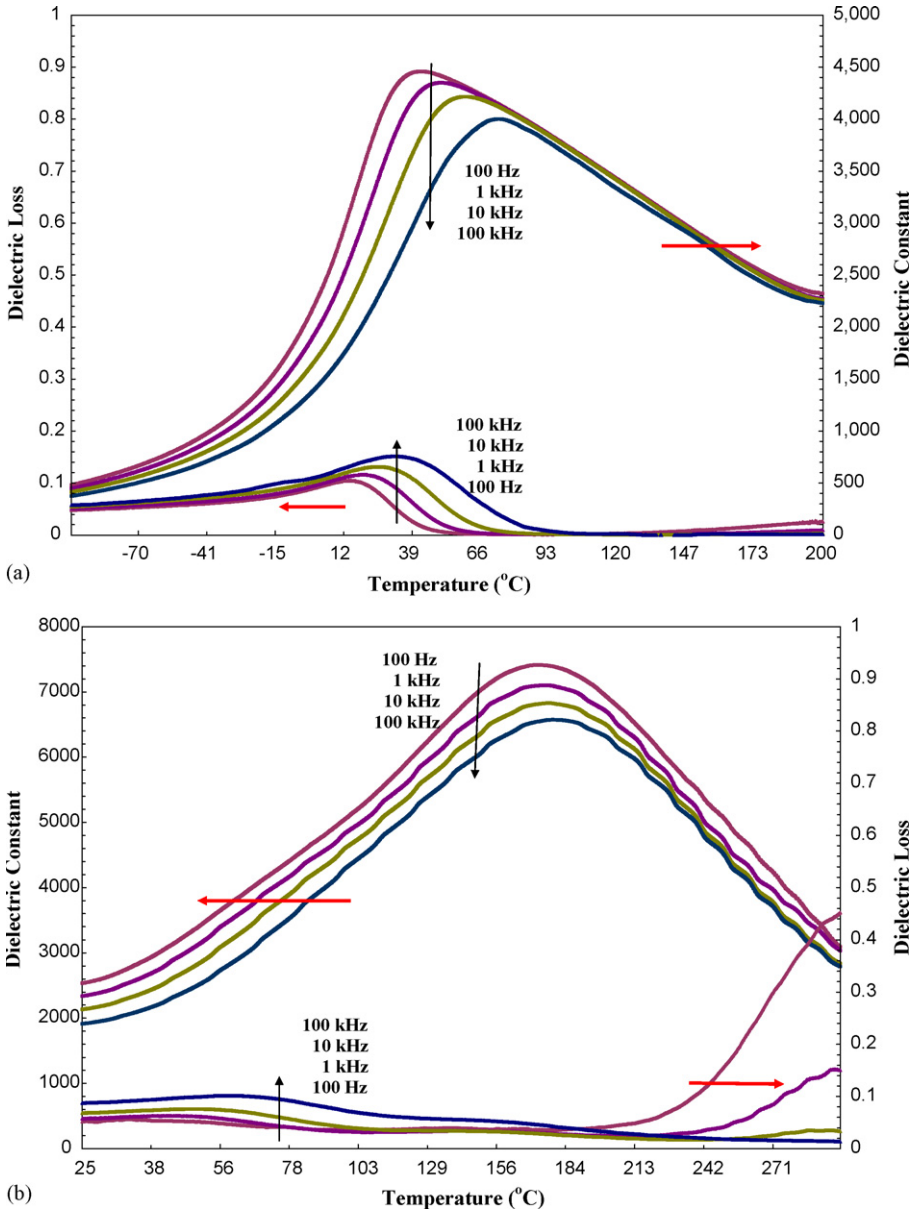

Fig. 3. (a) Temperature and frequency dependences of dielectric properties of PIN ceramic. (b) Temperature and frequency dependences of dielectric properties of 0.9PIN–0.1PT ceramic. (c) Temperature and frequency dependences of dielectric properties of 0.8PIN–0.2PT ceramic. (d) Temperature and frequency dependences of dielectric properties of 0.7PIN–0.3PT ceramic. (e) Temperature and frequency dependences of dielectric properties of 0.6PIN–0.4PT ceramic. (f) Temperature and frequency dependences of dielectric properties of 0.5PIN–0.5PT ceramic.

Please cite this article in press as: S. Wongsaenmai et al., J. Alloys Compd. (2007), doi:10.1016/j.jallcom.2006.12.053

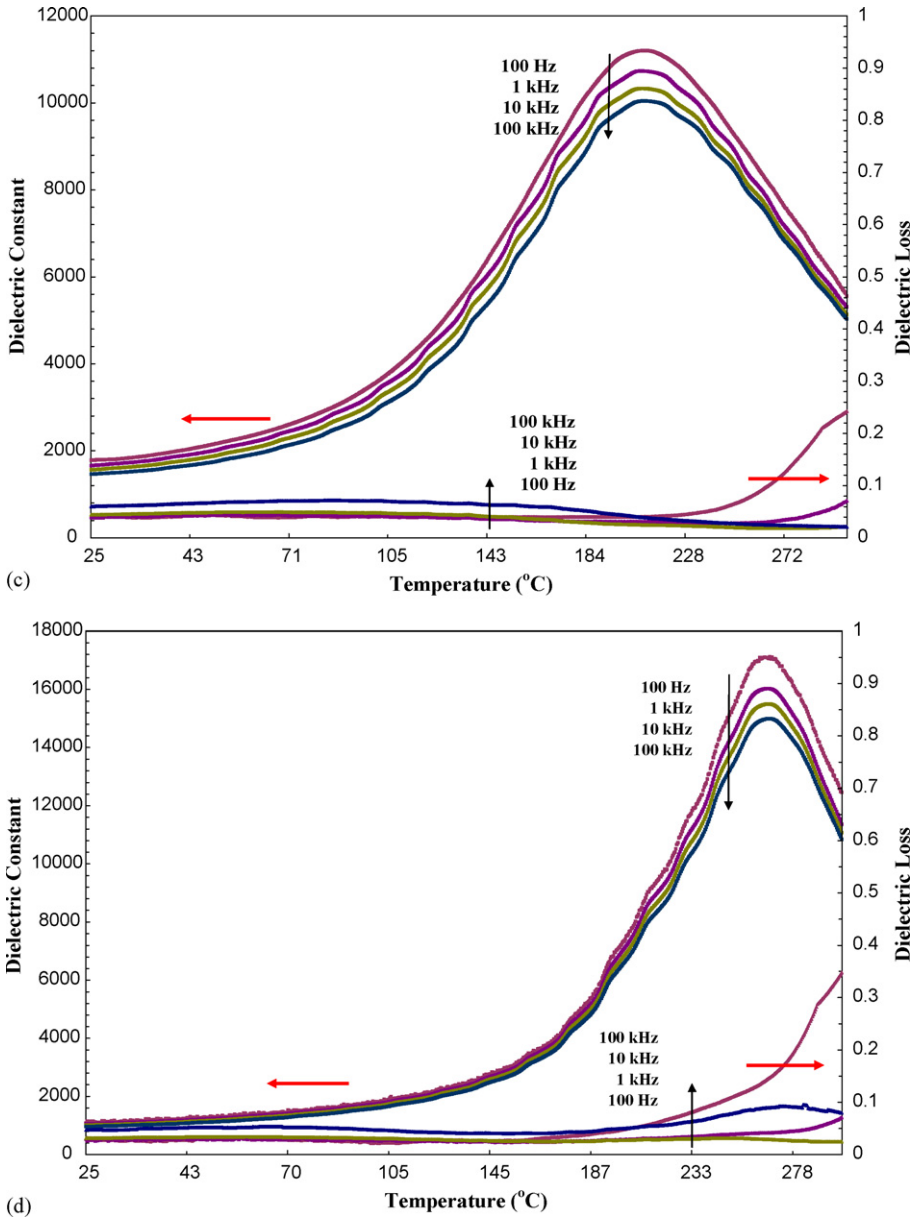

Fig. 3. (*Continued*)

as a result of thermally activated space charge conduction [26].

The dielectric properties of PIN ceramic, as plotted in Fig. 3(a), change significantly with temperature and frequency. Both dielectric constant (ε_r) and dielectric loss tangent ($\tan\delta$) exhibit strong temperature-frequency dependence below the transition temperature, indication of a typical relaxor ferroelectric behavior. In this case, the temperatures of maximum dielectric constant and dielectric loss tangent are shifted to higher temperature with increasing frequency. The maximum value of the dielectric constant decreases with increasing frequency, while that of the dielectric loss tangent increases. The dielectric properties then become frequency independence above the transition temperature [2,26]. While PIN exhibits a relaxor ferroelectric behavior, PT is a normal ferroelectric with nearly frequency-independent dielectric properties [27]. When PT is added to form the binary system with PIN, the dielectric behavior of PIN–PT should shift towards that of normal ferroelectric materials. As seen in Fig. 3(b)–(f), the dielectric properties exhibit a mixture of both normal and relaxor characteristics, in which the transition temperature is not shifted with frequency as much as for the PIN ceramic and the dielectric properties exhibit weaker temperature-frequency dependence below the transition temperature. This frequency dispersion in the dielectric properties can be quantified with $\Delta T = T_{m,100\,kHz} - T_{m,100\,Hz}$, which can be used as a rough estimate for more relaxor behavior with higher ΔT. As listed in Table 1, an addition of PT results in smaller ΔT. These results indicate the decreasing of relaxor behavior with increasing PT content [28]. Consequently, the dielectric peaks have become sharper with increasing PT content. Similar tendency has also been observed in several prior investigations [4–7,9,11].

Please cite this article in press as: S. Wongsaenmai et al., J. Alloys Compd. (2007), doi:10.1016/j.jallcom.2006.12.053

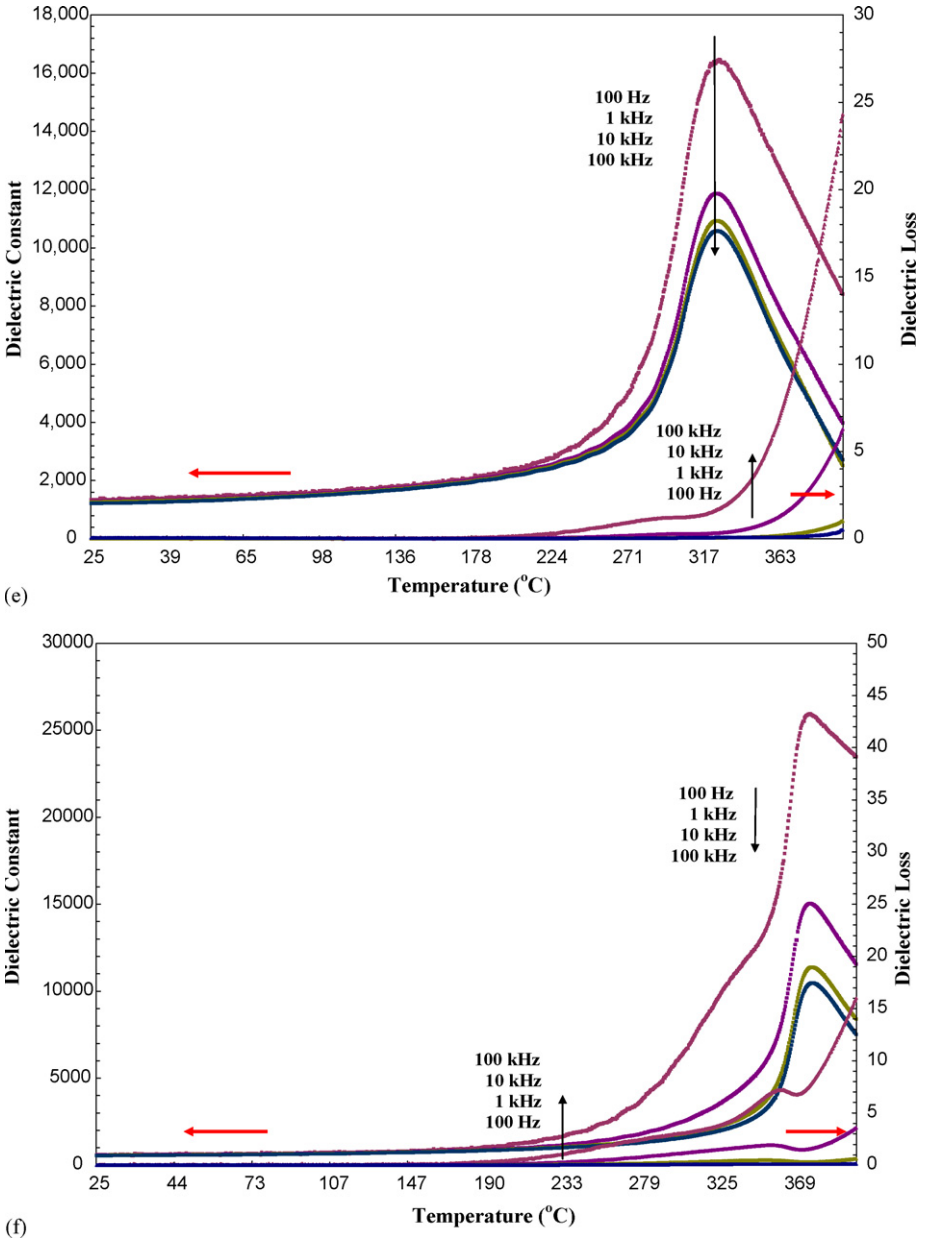

Fig. 3. (*Continued*).

The degree of broadening or diffuseness in the observed dielectric variation could also be estimated with the diffusivity (γ) using the expression $\ln(1/\varepsilon_r - 1/\varepsilon_{max})$ versus $(T - T_{max})^{\gamma}$. The value of γ can vary from 1, for normal ferroelectrics with a normal Curie–Weiss behavior, to 2, for completely disordered relaxor ferroelectrics [6,26]. The values of γ listed in Table 1 vary between 1.89 and 1.62, which confirms that diffuse phase transitions (DPT) occur in PIN–PT ceramics with a high degree of disorder. This observation clearly quantifies the decreasing of relaxor behavior with increasing PT content, as discussed earlier. Decreasing trend of γ value with increasing of PT content observed in PIN–PT system agrees with the previous study [29].

The dependence of temperature of maximum dielectric constant (T_m) on frequency of PIN–PT system can be explained with Vogel–Fulcher equation:

$$\varpi = f_0 \exp\left[\frac{-E_a}{k(T_m - T_f)}\right] \quad (1)$$

where f_0, E_a and T_f are the Debye frequency, the activation energy and the static freezing temperature, respectively [30]. The Debye frequency, the activation energy and the static freezing temperature obtained by fitting the experimental data with Eq. (1) are listed in Table 2. From Eq. (1), it is known that the activation energy is an internal energy of the cluster, which concerns with an anisotropy energy, K_{anis} and the cluster volume, V [31]. The fitting results show that the activation energy increases with increasing PT content for PIN–PT system, indicating that PT induces the increasing of the anisotropy energy and the cluster

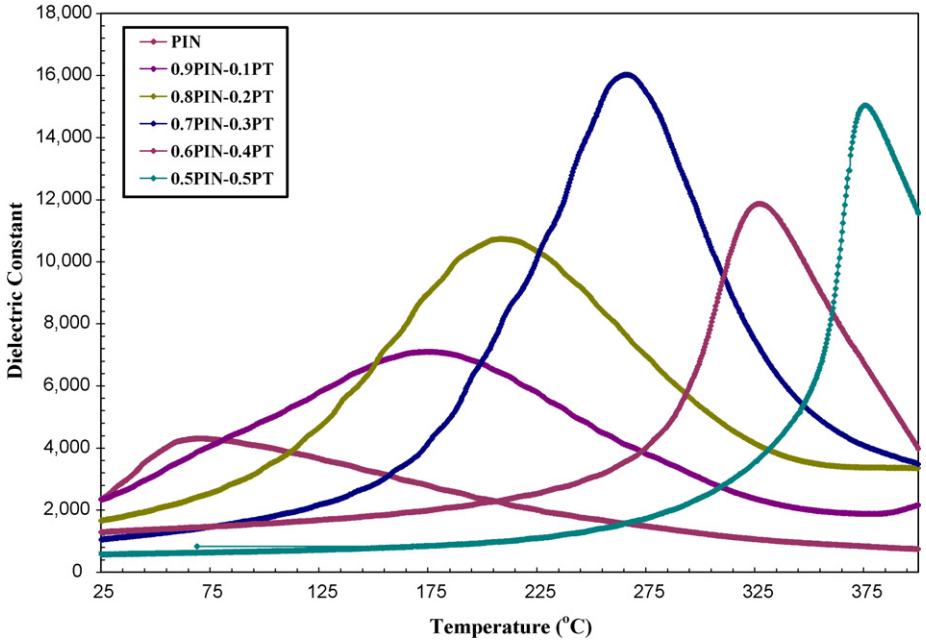

Fig. 4. Temperature dependence of dielectric constant of $(1-x)$PIN–xPT ceramics (measured at 1 kHz).

volume. It can be implied that size of isolated cluster or ordering increase with increasing PT contents [30,31]. For relaxor ferroelectrics, the value of Debye frequency concerns with size of polar nano-region and interaction between polar nano-regions [30]. In general, the stronger interaction and larger size show the smaller of the Debye frequency value [31]. Therefore, it can be implied that the increasing PT content shows marked effect in decreasing relaxor behavior by increasing size of and interaction between polar nano-regions, in good agreement with the observations discussed earlier. Similar observation has also been reported in other relaxor-based systems [32].

Fig. 5 illustrates a series of polarization (P–E) hysteresis loops for the PIN–PT ceramics. It is clearly evident that the shape of P–E loops varies greatly with the ceramic compositions. The hysteresis curve of PIN ceramic is of a "slim" loop type, a characteristic of the suppressed ferroelectric interaction [2,26]. This is typically found in the relaxor ferroelectrics with polar nano-regions. The hysteresis loops of PIN–PT ceramics become more developed showing large remnant polarization (P_r: remaining polarization when electric field is decreased to zero) and large saturated polarization (P_s) with increasing PT content up to 30 mol%. The hysteresis loops are of a typical "square" form as a result of domain switching in an applied field. This is a typical characteristic of a phase that contains long-range interaction between dipoles in the ferroelectric micro-domain state [26]. From the loops, the polarizations (P_r and P_s) and the coercive field E_C (indicating an electric field required to zero the polarization) are determined and listed in Table 3. In addition, the ferroelectric characteristic of the ceramics can be assessed with the hysteresis loop squareness (R_{sq}) which is typically understood to be the ratio of P_r/P_s where P_r is the remnant polarization at zero electric field and P_s is the saturated polarization obtained at some finite field strength below the dielectric breakdown. Jin et al. [33] used the loop squareness to measure not only the deviation in the polarization axis but also that in the electric field axis with the empirical expression $R_{sq} = (P_r/P_s) + (P_{1.1E_c}/P_r)$, where $P_{1.1E_c}$ is the polarization at the field equal to $1.1E_c$. For the ideal square loop, R_{sq} is equal to 2.00. As listed in Table 3, the value of R_{sq} increases with increasing PT content up to 30 mol%.

These results clearly indicate that an addition of PT induces the normal ferroelectric behaviors of PT into the PIN–PT ceramic system. More interestingly, it should also be noticed that a conclusion drawn from the XRD analysis and dielectric properties measurements discussed earlier that the MPB composition should exist between $x = 0.3$ and 0.4 is supported further

Table 2
The parameters obtained from fitting Vogel–Fulcher equation for $(1-x)$PIN–xPT ceramics

x	T_f (K)	f_0 (Hz)	E_a (eV)
0.0	310	3.9×10^{10}	0.042
0.1	434	3.0×10^{10}	0.015
0.2	471	2.8×10^{10}	0.010
0.3	535	2.6×10^{10}	0.004
0.4	599	2.3×10^{10}	0.002
0.5	649	1.4×10^{10}	0.001

Table 3
Ferroelectric properties of $(1-x)$PIN–xPT ceramics

x	Ferroelectric properties (at 25 °C)			Loop squareness (R_{sq})
	P_r (μC/cm^2)	P_s (μC/cm^2)	E_C (kV/cm)	
0.0	–	–	–	–
0.1	6.46	14.25	6.57	0.73
0.2	15.52	19.63	9.47	1.31
0.3	20.43	27.05	8.58	0.97
0.4	5.65	11.99	11.68	0.59
0.5	1.28	3.75	8.70	0.46

Please cite this article in press as: S. Wongsaenmai et al., J. Alloys Compd. (2007), doi:10.1016/j.jallcom.2006.12.053

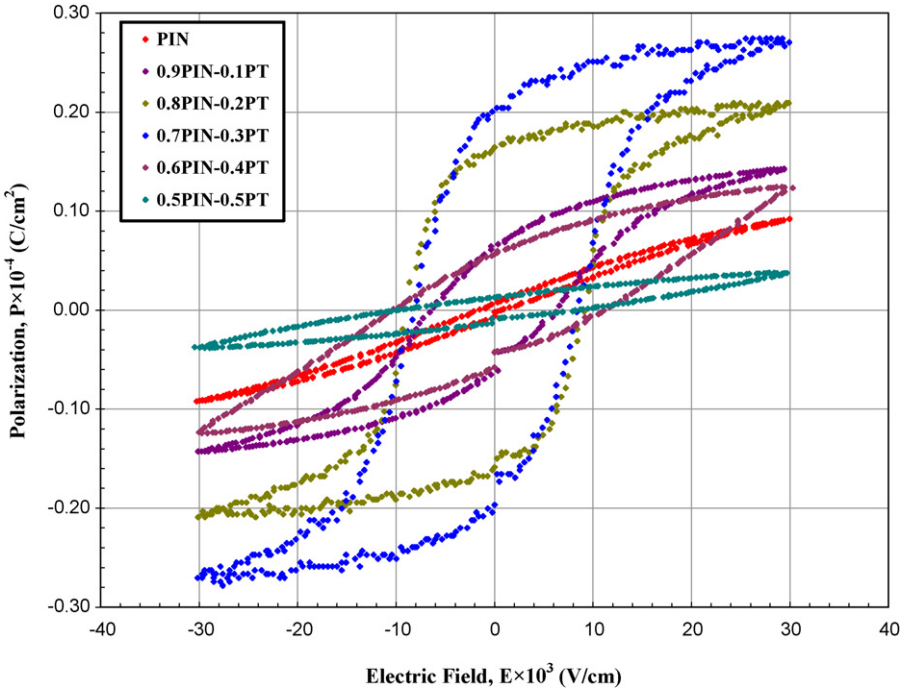

Fig. 5. *P–E* hysteresis loops of $(1-x)$PIN–xPT ceramics.

by the ferroelectric properties, as seen from a strong enhancement of polarization values with increasing PT content up to $x=0.3$, then a sudden drop of the polarization values with further increase in PT content. Finally, it is worthy noting that the fine grains PIN–PT ceramics obtained via the vibro-milling technique used in this study yield slightly better dielectric properties than the coarse grains PIN–PT ceramics in previous investigations [10–13]. However, as only very few investigations have been performed on PIN–PT ceramics, further investigations are still needed for more thoroughly and better comparison.

4. Conclusion

The $(1-x)Pb(In_{1/2}Nb_{1/2})O_3$–$xPbTiO_3$ (when $x=0.1$, 0.2, 0.3, 0.4, and 0.5) ceramics were prepared by an oxide-mixing method via a vibro-milling technique. The dielectric properties of the ceramics were determined as functions of both temperature and frequency with an automated dielectric measurement system, while the room temperature ferroelectric properties were measured by means of a standardized ferroelectric test system. The dielectric measurement took place over the temperature range of 25 and 400 °C with measuring frequency between 100 Hz and 100 kHz. Fine grains ceramics were achieved with average grain size of 1–2 μm, indicating advantage of the vibro-milling technique used. The results indicated that the dielectric properties of PIN ceramic were of relaxor ferroelectric behavior. The dielectric properties of PIN–PT ceramics showed a mixed relaxor and normal ferroelectric behavior, with more normal ferroelectric behavior observed with increasing PT content. The *P–E* hysteresis loop measurements demonstrated that the ferroelectric properties of the ceramics in PIN–PT system changed from the relaxor ferroelectric behavior in PIN ceramic to the normal ferroelectric behavior in PIN–PT ceramics. These results clearly show the significance of the added PT in reducing the relaxor ferroelectric behavior in PIN ceramic. More interestingly, XRD analysis, and dielectric and ferroelectric properties measurements also indicated the existence of the MPB composition between $x=0.3$ and 0.4. Finally, the fine grains PIN–PT ceramics showed slightly better dielectric properties than the coarse grains ceramics in previous investigations.

Acknowledgments

The authors would like to express their gratitude for financial supports from the Thailand Research Fund (TRF), Commission on Higher Education (CHE), Graduate School and Faculty of Science of Chiang Mai University, and Ministry of University Affairs in Thailand.

References

[1] K. Uchino, Ferroelectric Devices, Marcel Dekker, New York, 2000.
[2] G.H. Haertling, J. Am. Ceram. Soc. 82 (1999) 797–818.
[3] L.E. Cross, Mater. Chem. Phys. 43 (1996) 108–115.
[4] S.E. Park, T.R. Shrout, J. Appl. Phys. 82 (1997) 1804–1811.
[5] J. Kuwata, K. Uchino, S. Nomura, Jpn. J. Appl. Phys. 21 (1982) 1298–1302.
[6] R. Yimnirun, Int. J. Mod. Phys. B, in press.
[7] G. Xu, H. Luo, Y. Guo, Y. Gao, H. Xu, Z. Qi, W. Zhong, Z. Yin, Solid State Commun. 120 (2001) 321–324.
[8] N. Yasuda, H. Ohwa, M. Kume, Y. Yamashita, Jpn. J. Appl. Phys. 39 (2000) 5586–5588.
[9] N. Yasuda, H. Ohwa, D. Hasegawa, H. Hosono, Y. Yamashita, M. Iwata, Y. Ishibashi, Ferroelectrics 270 (2002) 247–252.
[10] M. Pham-Thi, C. Augier, H. Dammak, P. Gaucher, Ultrasonics 44 (2006) e627–e631.
[11] C. Augier, M. Pham-Thi, H. Dammak, P. Gaucher, J. Eur. Ceram. Soc. 25 (2005) 2429–2432.

[12] Y. Guo, H. Luo, T. He, Z. Yin, Solid State Commun. 123 (2002) 417–420.
[13] E.F. Alberta, A.S. Bhalla, J. Phys. Korea 32 (1998) s1265–s1269.
[14] N. Yasuda, M. Sakaguchi, Y. Itoh, H. Ohwa, Y. Yamashita, M. Iwata, Y. Ishibashi, Jpn. J. Appl. Phys. 42 (2003) 6205–6208.
[15] N. Yasuda, H. Ohwa, M. Kume, K. Hayashi, Y. Hosono, Y. Yamashita, J. Cryst. Growth 229 (2001) 299–304.
[16] B. Jaffe, W.R. Cook, H. Jaffe, Piezoelectric Ceramics, Academic Press, New York, 1971.
[17] Y.H. Xu, Ferroelectric Materials and their Applications, North Holland, Los Angeles, 1991.
[18] R. Wongmaneerung, R. Yimnirun, S. Ananta, Mater. Lett. 60 (2006) 2666–2671.
[19] R. Wongmaneerung, T. Sarnkonsri, R. Yimnirun, S. Ananta, Mater. Sci. Eng. B 130 (2006) 246–253.
[20] A. Ngamjarurojana, O. Khamman, R. Yimnirun, S. Ananta, Mater. Lett. 60 (2006) 2867–2872.
[21] S. Wongsaenmai, R. Yimnirun, S. Ananta, Mater. Lett., in press.
[22] E.F. Alberta, A.S. Bhalla, Mater. Lett. 29 (1996) 127–129.
[23] R. Wongmaneerung, R. Yimnirun, S. Ananta, Mater. Lett. 60 (2006) 1447–1452.
[24] S. Wongsaenmai, R. Yimnirun, S. Ananta, J. Mater. Sci., in press.
[25] S. Wongsaenmai, O. Khamman, S. Ananta, R. Yimnirun, J. Electroceram., in press.
[26] L.E. Cross, Ferroelectrics 76 (1987) 241–267.
[27] R. Wongmaneerung, R. Yimnirun, S. Ananta, Appl. Phys. A 86 (2007) 249–255.
[28] C. Lei, K. Chen, X. Zhang, J. Wang, Solid State Commun. 123 (2002) 445–450.
[29] M. Kuwabara, S. Takahashi, K. Goda, K. Oshima, K. Watanabe, Jpn. J. Appl. Phys. 31 (1992) 3241–3244.
[30] D. Viehland, S.-J. Jang, L.E. Cross, J. Appl. Phys. 68 (1990) 2916–2921.
[31] D. Viehland, S.-J. Jang, L.E. Cross, M. Wutting, Phys. Rev. B 46 (1992) 8003–8006.
[32] G. Singh, V.S. Triwari, V.K. Waghawan, Solid State Commun. 129 (2004) 665–670.
[33] B.M. Jin, J. Kim, S.C. Kim, Appl. Phys. A 65 (1997) 53–56.

Please cite this article in press as: S. Wongsaenmai et al., J. Alloys Compd. (2007), doi:10.1016/j.jallcom.2006.12.053

Available online at www.sciencedirect.com
ScienceDirect
Materials Letters xx (2007) xxx–xxx
materials letters
www.elsevier.com/locate/matlet

Effect of calcination conditions on phase formation and particle size of $Zn_3Nb_2O_8$ powders synthesized by solid-state reaction

A. Prasatkhetragarn, R. Yimnirun, S. Ananta *

Department of Physics, Faculty of Science, Chiang Mai University, Chiang Mai 50200, Thailand

Received 19 October 2006; accepted 21 December 2006

Abstract

The solid-state mixed oxide method via a rapid vibro-milling technique is explored in the preparation of single-phase $Zn_3Nb_2O_8$ powders. The formation of the $Zn_3Nb_2O_8$ phase in the calcined powders has been investigated as a function of calcination conditions by TG–DTA and XRD techniques. Morphology, particle size and chemical composition have been determined via a combination of SEM and EDX techniques. It has been found that the minor phases of unreacted ZnO and Nb_2O_5 precursors and the columbite $ZnNb_2O_6$ phase tend to form together with the $Zn_3Nb_2O_8$ phase, depending on calcination conditions. It is seen that optimization of calcination conditions can lead to a single-phase $Zn_3Nb_2O_8$ in a monoclinic phase.

Keywords: $Zn_3Nb_2O_8$; Calcination; Phase formation; Particle size; Nanopowders

1. Introduction

The quest for optimal powder characteristics (controlled chemical composition, homogeneity, reactivity, particle size and shape) in the fabrication of materials has directed attention particularly towards powder production techniques. It is known that various compositions are possible in the Zn–Nb–O system [1,2]. To date, three possible zinc niobium oxides have been identified: $ZnNb_2O_6$, $Zn_2Nb_{34}O_{87}$ and $Zn_3Nb_2O_8$ [1,2]. Amongst these compounds, zinc niobate ($ZnNb_2O_6$) is one of the most well-known materials, which has recently gained considerable attention [3,4]. This compound is very well known as the key precursor for the successful preparation of single-phase perovskite lead zinc niobate, $Pb(Zn_{1/3}Nb_{2/3})O_3$, or PZN-based materials, which are becoming increasingly important for multilayer ceramic capacitor, electrostrictor and actuator applications [5,6]. In general, production of single-phase $ZnNb_2O_6$ is not straightforward, as a minor concentration of the ZnO is sometimes formed alongside the major phase of $ZnNb_2O_6$ [7,8].

In contrast, very little is known about $Zn_3Nb_2O_8$, since no work has been dedicated to the synthesis of this compound.

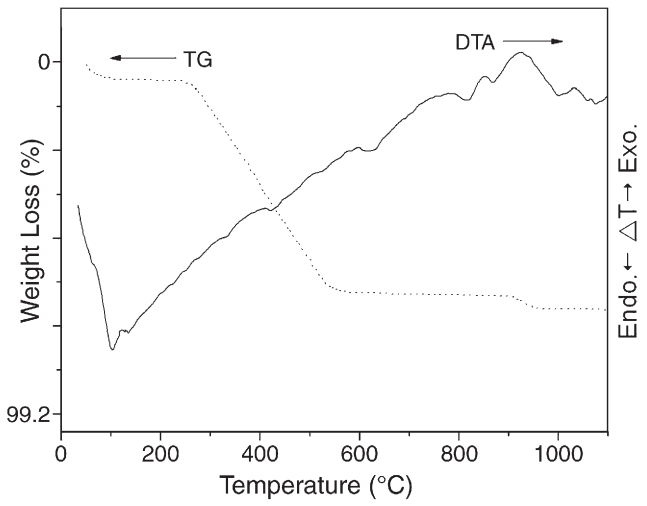

Fig. 1. TG–DTA curves for the mixture of $3ZnO–Nb_2O_5$ powder.

* Corresponding author. Tel.: +66 53 943367; fax: +66 53 943445.
E-mail address: Suponananta@yahoo.com (S. Ananta).

0167-577X/$ - see front matter © 2007 Published by Elsevier B.V.
doi:10.1016/j.matlet.2006.12.050

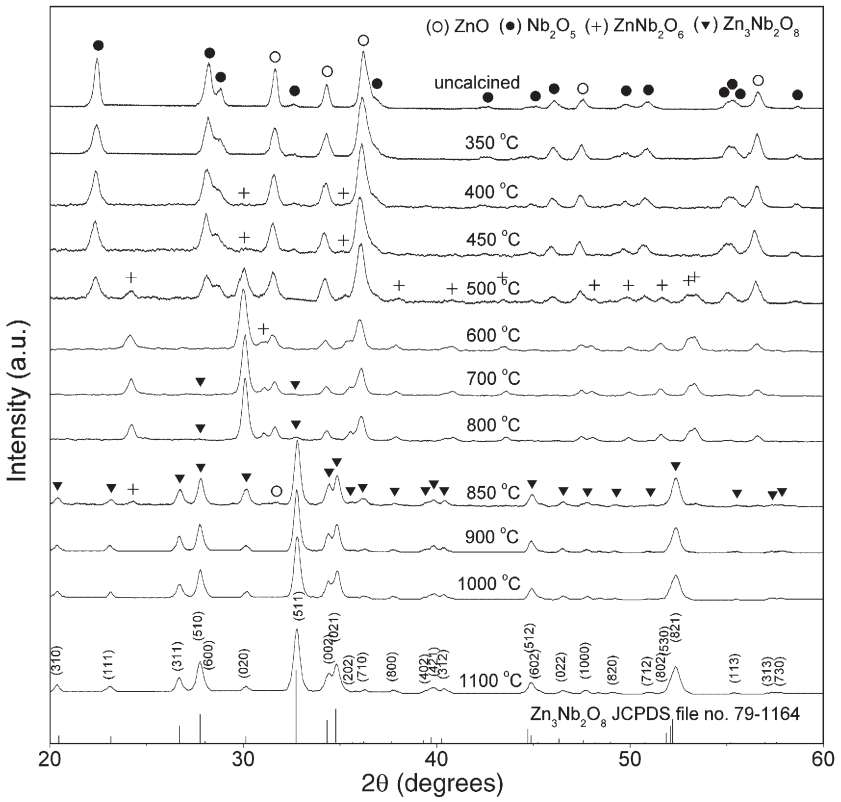

Fig. 2. XRD patterns of ZN powders calcined at various temperatures for 5 h with heating/cooling rates of 10 °C/min.

Much of the work concerning the $Zn_3Nb_2O_8$ compound has been directed towards determining crystal structure and microwave dielectric properties [9–11]. Kasper [10] and Isobe et al. [11] reported that the structure of $Zn_3Nb_2O_8$ is closely related to the columbite structure of $ZnNb_2O_6$. Its crystal structure can be represented as an order super-structure of α-PbO_2 [12]. Moreover, to date, the potential of $Zn_3Nb_2O_8$ as a possible alternative precursor for the preparation of PZN has not yet been reported. Interestingly, the mixed oxide route for the production of $Zn_3Nb_2O_8$ powders has not received detailed attention, and the effects of calcination conditions (*i.e.* applied firing temperature, dwell time and heating/cooling rates) have not yet been studied extensively. Therefore, the main purpose of this work was to explore a simple mixed oxide synthetic route

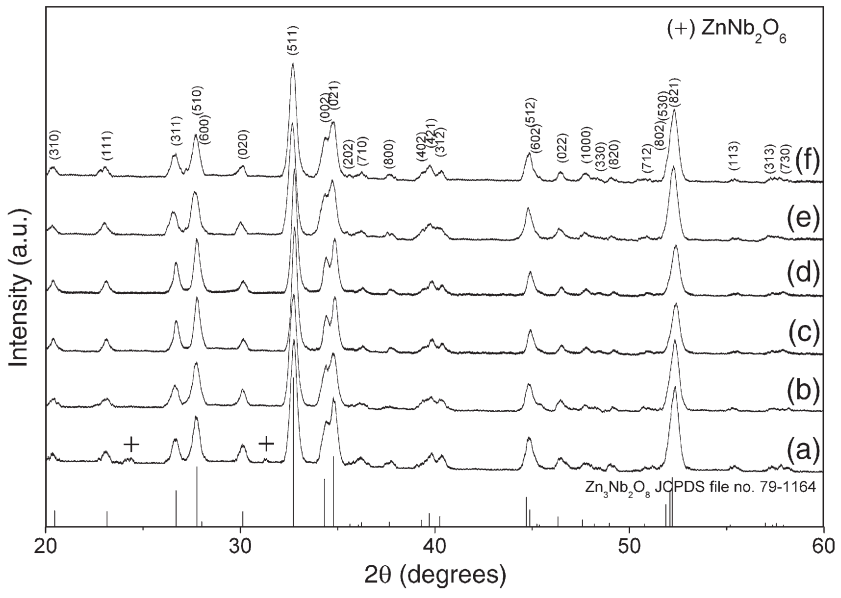

Fig. 3. XRD patterns of ZN powders calcined at 900 °C for (a) 0.5, (b) 1, (c) 2 and (d) 3 h, with heating/cooling rates of 10 °C/min and for 1 h with heating/cooling rates of (e) 20 and (f) 30 °C/min.

Please cite this article as: A. Prasatkhetragarn et al., Effect of calcination conditions on phase formation and particle size of $Zn_3Nb_2O_8$ powders synthesized by solid-state reaction, Mater. Lett. (2007), doi:10.1016/j.matlet.2006.12.050

for the production of $Zn_3Nb_2O_8$ powders via a rapid vibro-milling technique and to perform a systematic study of the reaction between the starting zinc oxide and niobium oxide precursors. The phase formation and morphology of the powder calcined at various conditions will be studied and discussed. The study also forms a possible basis for a further survey on PZN preparation.

2. Experimental procedure

The starting materials were commercially available zinc oxide, ZnO (JCPDS file number 89-1397) and niobium oxide, Nb_2O_5 (JCPDS file number 30-0873) (Aldrich, 99.9% purity). The two oxide powders exhibited an average particle size in the range 3.0–5.0 μm. $Zn_3Nb_2O_8$ powders were synthesized by the solid-state reaction of thoroughly ground mixtures of ZnO and Nb_2O_5 powders that were milled in the required stoichiometric ratio. In order to combine mixing capacity with a significant time saving, a McCrone vibro-milling technique [8,13] was carried out for 0.5 h with corundum cylindrical media in isopropyl alcohol (IPA). After drying at 120 °C for 2 h, the reaction of the uncalcined powders taking place during heat treatment was investigated by thermogravimetric and differential thermal analyses (TG–DTA, Shimadzu), using a heating rate of 10 °C/min in air from room temperature up to 1100 °C. Based on the TG–DTA results, the mixture was calcined at

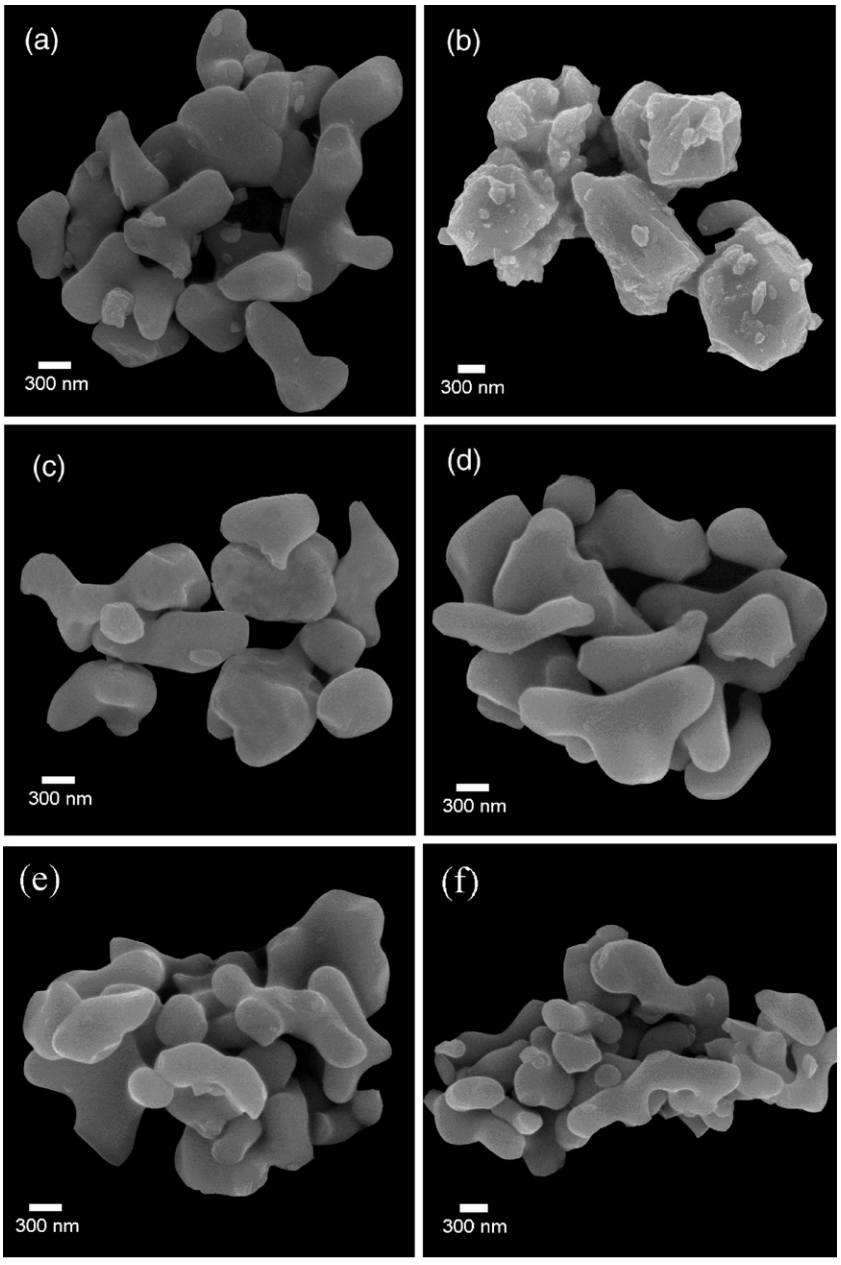

Fig. 4. SEM micrographs of ZN powders calcined for 1 h with heating/cooling rates of 10 °C/min at (a) 900 and (b) 1050 °C, and at 900 °C for (c) 3 and (d) 5 h; and at 900 °C for 1 h with heating/cooling rates of (e) 20 and (f) 30 °C/min.

Please cite this article as: A. Prasatkhetragarn et al., Effect of calcination conditions on phase formation and particle size of $Zn_3Nb_2O_8$ powders synthesized by solid-state reaction, Mater. Lett. (2007), doi:10.1016/j.matlet.2006.12.050

Table 1
Particle size range of $Zn_3Nb_2O_8$ powders calcined at various conditions

Calcination conditions			Particle size range	
Temperature (°C)	Dwell times (h)	Heating/cooling rates (°C/min)	SEM (±5 nm)	XRD (±0.05 nm)
900	1	10	60–1950	30.18
900	1	20	80–2130	31.11
900	1	30	110–2740	37.00
900	3	10	283–1988	35.31
900	5	10	313–2400	35.87
1050	1	10	80–2110	40.73

various conditions, in closed alumina crucible, in order to investigate the formation of $Zn_3Nb_2O_8$.

All powders were subsequently examined by room temperature X-ray diffraction (XRD; Siemens-D500 diffractometer), using Ni-filtered CuK_α radiation to identify the phases formed and optimum calcination conditions for the formation of $Zn_3Nb_2O_8$ powders. Powder morphologies and particle sizes were directly imaged, using scanning electron microscopy (SEM; JEOL JSM-840A). The chemical compositions of the phase formed were elucidated by an energy-dispersive X-ray (EDX) analyzer with an ultra-thin window. EDX spectra were quantified with the virtual standard peaks supplied with the Oxford Instruments eXL software.

3. Results and discussion

The TG–DTA simultaneous analysis of a powder mixed in the stoichiometric proportions of $Zn_3Nb_2O_8$ is displayed in Fig. 1. In the temperature range from room temperature to ~150 °C, the sample shows both exothermic and endothermic peaks in the DTA curve, consistent with the first weight loss. These observations can be attributed to the decomposition of the organic species such as rubber lining from the milling process similar to our earlier reports [8,13]. Corresponding to the second fall in sample weight, by increasing the temperature further to ~400 °C, a slight thermal fluctuation in the DTA curve is observed. This may be attributed to the crystallization of $ZnNb_2O_6$ as reported earlier [8]. Increasing the temperature up to ~1100 °C, the solid-state reaction occurred between ZnO and Nb_2O_5 [8,14]. The broad exotherm with several peaks in the DTA curve represents that reaction, which has maxima at ~830 °C and 900 °C. These are supported by the third falls in sample weight over the same temperature ranges. However, it is to be noted that there is no obvious interpretation of these peaks, although it is likely to correspond to a phase transition reported earlier [1,8,14]. These data were used to define the range of calcination temperatures for XRD investigation between 350 and 1100 °C.

To further study the phase development with increasing calcination temperature in the powders, they were calcined for 5 h in air at various temperatures, up to 1100 °C, followed by phase analysis using XRD. As shown in Fig. 2, for the uncalcined powders and the powders calcined at 350 °C, only X-ray peaks of precursors ZnO (○) and Nb_2O_5 (●), which could be matched with JCPDS file numbers 89-1397 [15] and 30-0873 [16], respectively, are present, indicating that no reaction had yet been triggered during the vibro-milling and low firing processes. However, it is seen that a small portion of the crystalline phase of the $ZnNb_2O_6$ crystallites (+) as reported by Ngamjarurojana et al. [8] was found as separated phases in the powders calcined at 400 °C, and became the predominant phase in the powder calcined above 450 °C. As the temperature increased to 800 °C, the intensity of the $ZnNb_2O_6$ peaks was further enhanced whereas some new peaks (▼) of the desired $Zn_3Nb_2O_8$ phase, started to appear, mixing with the $ZnNb_2O_6$ and ZnO phases after calcinations above 600 °C. These observations are associated with the DTA peaks found at the same temperature range within the broad exothermic effects in Fig. 1. In a first approximation, this $ZnNb_2O_6$ phase has a columbite-type structure with an orthorhombic unit cell (a=1420.8 pm, b=572.6 pm and c=504.0 pm, space group *Pbcn* (no. 60)), consistent with JCPDS file number 76-1827 [17]. This observation could be attributed mainly to the poor reactivity of zinc and niobium species [8]. Upon calcination at 900 °C, a single phase of $Zn_3Nb_2O_8$ is already formed. For the present work, there are no significant differences between the powders calcined at temperatures ranging from 900 to 1100 °C. This $Zn_3Nb_2O_8$ phase (JCPDS file number 79-1164 [18]) has a corundum structure with a monoclinic unit cell (a=1909.3 pm, b=592.7 pm and c=522.0 pm, space group *C2/c* (no. 15)), in agreement with the literature [11].

Apart from the calcination temperature, the effect of dwell time was also found to be quite significant. From Fig. 3, it can be seen that the single phase of $Zn_3Nb_2O_8$ (yield of 100% within the limitations of the XRD technique) was found to be possible in powders calcined at 900 °C with dwell time of at least 1 h (Fig. 3(a–d)) applied. This is probably due to the effectiveness of vibro-milling and a carefully optimized reaction. The observation that the dwell time may also play an important role in obtaining a single-phase corundum product is also consistent with other similar systems [8,19]. It is also very interesting to see that the on-set temperature is approximately 200–250 °C lower than that reported earlier with a conventional ball-milling method [9,14]. The difference could be attributed to nano-sized mixed powders obtained from a rapid vibro-milling. Most importantly, this study suggests that a rapid vibro-milling method can significantly lower the optimum calcination temperature for formation of single-phase $Zn_3Nb_2O_8$ powders.

In the present study, an attempt was also made to calcine $Zn_3Nb_2O_8$ powders under various heating/cooling rates (Fig. 3(b, e and f)). In this connection, it is shown that faster heating/cooling rates can also lead to crystallization of the $Zn_3Nb_2O_8$ phase. Based on the TG–DTA and XRD data, it may be concluded that, over a wide range of calcination conditions, a single phase of $Zn_3Nb_2O_8$ cannot be straightforwardly formed via a solid-state mixed oxide synthetic route, unless a careful design of calcination is performed. The experimental work carried out here suggests that the optimal calcination conditions for single-phase $Zn_3Nb_2O_8$ (with impurities undetected by XRD technique) are 900 °C for 1 h with heating/cooling rates as fast as 30 °C/min. Moreover, the formation temperature and dwell time for the production of $Zn_3Nb_2O_8$ powders observed in this work are also much lower than those reported

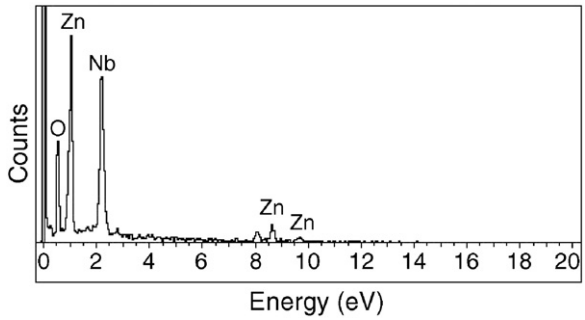

Fig. 5. EDX analysis of the $Zn_3Nb_2O_8$ powders.

Please cite this article as: A. Prasatkhetragarn et al., Effect of calcination conditions on phase formation and particle size of $Zn_3Nb_2O_8$ powders synthesized by solid-state reaction, Mater. Lett. (2007), doi:10.1016/j.matlet.2006.12.050

earlier [9,14]. This clearly emphasizes the advantages of a rapid vibro-milling technique.

Finally, the morphological changes in the $Zn_3Nb_2O_8$ powders formed by a mixed oxide are illustrated in Fig. 4(a–f) as a function of calcination temperatures, dwell times and heating/cooling rates, respectively. The influence of calcination conditions on particle size is given in Table 1. In general, the particles are agglomerated and irregular in shape, with a substantial variation in particle size, particularly in samples calcined at high temperature (Fig. 4(b)) or with fast heating/cooling rates (Fig. 4(e, f)). This finding is also similar to that in $ZnNb_2O_6$ and $ZrTiO_4$ powders [8,20]. The results indicate that calculated crystalline size and degree of agglomeration tend to increase with calcination temperatures or heating/cooling rates (Table 1). All powders seem to display a significant level of necking and bonding as if they were in the initial stages of sintering. This observation could be attributed to the mechanism of surface energy reduction of the ultrafine powders, *i.e.* the smaller the powder the higher the specific surface area [21]. To the authors' knowledge, the present data are the first results for the morphology–calcination relationship of $Zn_3Nb_2O_8$ powders prepared by the solid-state reaction. It is also of interest to point out that mass production of single-phase $Zn_3Nb_2O_8$ nanopowders with the smallest particle size of ~60 nm (estimated from SEM micrographs) can be achieved by employing a simple solid-state reaction combined with a rapid vibro-milling technique. In addition, EDX analysis using a 20 nm probe on a large number of particles of the calcined powders confirms that the parent composition is $Zn_3Nb_2O_8$ (Fig. 5), in good agreement with XRD results.

4. Conclusions

The potential of a rapid vibro-milling technique as a significant time saving method to obtain single-phase $Zn_3Nb_2O_8$ nanopowders at low calcination temperatures has been demonstrated. The calcination conditions have been found to have a pronounced effect on both phase formation and particle size of the calcined $Zn_3Nb_2O_8$ powders. The resulting $Zn_3Nb_2O_8$ powders consist of a variety of agglomerated particle sizes, depending on the calcination conditions.

Acknowledgements

This work was supported by the Thailand Research Fund (TRF), the Commission on Higher Education (CHE), the Faculty of Science and the Graduate School, Chiang Mai University.

References

[1] A.J. Pollard, J. Am. Ceram. Soc. 44 (1961) 630.
[2] R.R. Dayal, J. Less-Common Met. 26 (1972) 381.
[3] R.C. Pullar, J.D. Breeze, N.M. Alford, J. Am. Ceram. Soc. 88 (2005) 2466.
[4] Y.C. Zhang, Z.X. Yue, Z.L. Gui, L.T. Li, Ceram. Int. 29 (2003) 555.
[5] J. Wang, W. Dongmei, X. Junmin, N.W. Beng, J. Am. Ceram. Soc. 82 (1999) 477.
[6] A.J. Moulson, J.M. Herbert, Electroceramics, 2nd ed.Wiley, Chichester, 2003.
[7] C.L. Li, C.C. Chou, Int. Ferro., vol. 55, 2003, p. 955.
[8] A. Ngamjarurojana, O. Khamman, R. Yimnirun, S. Ananta, Mater. Lett. 60 (2006) 2867.
[9] D.W. Kim, J.H. Kim, J.R. Kim, K.S. Hong, Jpn. J. Appl. Phys. 40 (2001) 5994.
[10] H. Kasper, Z. Anorg, Allg. Chem. 355 (1967) 1.
[11] M. Isobe, F. Marumo, S.I. Iwai, Y. Kondo, Bull. Tokyo Inst. Technol. 120 (1974) 1.
[12] F. Laves, G. Bayer, A. Panagos, Schweiz. Mineral. Petrogr. Mitt. 43 (1963) 217.
[13] R. Wongmaneerung, R. Yimnirun, S. Ananta, Mater. Lett. 60 (2006) 1447.
[14] Y.C. Lee, C.H. Lin, I.N. Lin, Mater. Chem. Phys. 79 (2003) 124.
[15] Powder Diffraction File No. 89-1397, International Centre for Diffraction Data, Newton Square, PA, 2000.
[16] Powder Diffraction File No. 30-0873, International Centre for Diffraction Data, Newton Square, PA, 2000.
[17] Powder Diffraction File No. 76-1827, International Centre for Diffraction Data, Newton Square, PA, 2000.
[18] Powder Diffraction File No. 79-1164, International Centre for Diffraction Data, Newton Square, PA, 2000.
[19] S. Ananta, Mater. Lett. 58 (2004) 2530.
[20] S. Ananta, R. Tipakontitikul, T. Tunkasiri, Mater. Lett. 57 (2003) 2637.
[21] J.S. Reed, Principles of Ceramic Processing, 2nd ed.Wiley, New York, 1995.

Please cite this article as: A. Prasatkhetragarn et al., Effect of calcination conditions on phase formation and particle size of $Zn_3Nb_2O_8$ powders synthesized by solid-state reaction, Mater. Lett. (2007), doi:10.1016/j.matlet.2006.12.050

J Mater Sci
DOI 10.1007/s10853-006-0404-1

Influence of calcination conditions on phase formation and particle size of indium niobate powders synthesized by the solid-state reaction

S. Wongsaenmai · R. Yimnirun · S. Ananta

Received: 4 November 2005 / Accepted: 2 May 2006

Abstract A wolframite-type phase of indium niobate, $InNbO_4$, has been synthesized by a solid-state reaction via a rapid vibro-milling technique. The formation of the $InNbO_4$ phase in the calcined powders has been investigated as a function of calcination conditions by TG-DTA and XRD techniques. Morphology, particle size and chemical composition have been determined via a combination of SEM and EDX techniques. Single-phase $InNbO_4$ powders have been obtained successfully for calcination condition of 900 °C for 4 h or 950 °C for 2 h with heating/cooling rates of 30 °C/min. Higher temperatures and longer dwell times clearly favoured particle growth and the formation of large and hard agglomerates.

Introduction

Indium niobate ($InNbO_4$, IN) is one of the binary niobate compounds with a wolframite crystal structure [1]. Earlier works concerning the $InNbO_4$ have been directed towards determining low-temperature dielectric [2], luminescent [3] and photocatalytic [4] properties. Recently, this compound is also a potential material for the development of photocatalytic systems capable of splitting water into H_2 and O_2 under visible light irradiation [5–7]. Moreover, it is well established as a key precursor for the partially successful preparation of single-phase ferroelectric perovskite lead indium niobate $Pb(In_{1/2}Nb_{1/2})O_3$ (PIN)-based ceramics, which is becoming increasingly important for actuator, transducer and ultrasonic motor applications [8, 9].

There has been a great deal of interest in the preparation of single-phase PIN powders as well as in the phase transition, ordering behaviour and electrical properties of PIN-based ceramics [10–18]. In general, the constituents In_2O_3 and Nb_2O_5 are first mixed and reacted together to form indium niobate ($InNbO_4$), prior to mixing and reacting with PbO in the second step of calcination at elevated temperature. Interestingly, this mixed oxide route has been employed with minor modifications in the synthesis of $InNbO_4$ itself [13–16]. However, powders prepared by a mixed oxide route have spatial fluctuations in their compositions. The extent of the fluctuations depends on the characteristics of the starting powders as well as on the processing schedule. Generally, the mixed oxide method involves the heating of a mixture of indium oxide and niobium oxide above 1,000 °C for long times i.e. 4 h [10, 13], 12 h [6], 24 h [14–17] and 48 h [4, 7]. The optimization of calcination conditions used in the mixed oxide process, however, has not received detailed attention, and the effects of applied dwell time and heating/cooling rates have not yet been studied extensively.

Therefore, the main purpose of this work is to explore a simple mixed oxide synthetic route for the production of $InNbO_4$ powders via a rapid vibro-milling technique and to perform a systematic study of the reaction between the starting indium oxide and niobium oxide precursors. The phase formation and morphology of the powders calcined at various conditions will be studied and discussed. The rapid vibro-milling technique is

S. Wongsaenmai · R. Yimnirun · S. Ananta (✉)
Department of Physics, Faculty of Science, Chiang Mai University, Chiang Mai 50200, Thailand
e-mail: Supon@chiangmai.ac.th

employed to explore the potentiality in obtaining nano-sized powders, which would in turn lead to lower required firing temperature.

Experimental procedure

The starting materials were commercially available indium oxide, In_2O_3 (JCPDS file number 71-2195) and niobium oxide, Nb_2O_5 (JCPDS file number 30-873) (Aldrich, 99.9% purity). The two oxide powders exhibited an average particle size in the range of 1.0–3.0 μm. $InNbO_4$ powders were synthesized by the solid-state reaction of thoroughly ground mixtures of In_2O_3 and Nb_2O_5 powders that were milled in the required stoichiometric ratio. Instead of employing a ball-milling procedure [10, 16], a McCrone vibro-milling technique was used [19, 20]. In this technique, a vibratory laboratory mill (McCrone Micronizing Mill) powered by a 1/30 HP motor was employed. The grinding vessel consists of a 125 mL capacity polypropylene jar fitted with a screw-capped, gasketless, polythene closure. The jar is packed with an ordered array of identical, cylindrical, grinding media of polycrystalline corundum. A total of 48 milling media with a powder weight of 20 g was kept constant in each batch. The milling operation was carried out in isopropanal inert to the polypropylene jar. In order to combine mixing capacity with a significant time saving, the milling operation was carried out for 0.5 h with corundum cylindrical media in isopropyl alcohol (IPA). After drying at 120 °C for 2 h, the reaction of the uncalcined powders taking place during heat treatment was investigated by themogravimetric and differential thermal analysis (TG-DTA, Shimadzu), using a heating rate of 10 °C/min in air from room temperature up to 1,000 °C. Based on the TG-DTA results, the mixture (~10 g for each batch) was calcined at various conditions, i.e. temperatures ranging from 700 °C to 1,200 °C, dwell times ranging from 0.5 h to 4 h and heating/cooling rates ranging from 3 °C/min to 30 °C/min, in closed alumina crucible [cylindrical shape with 25 mL capacity (3 cm in diameter and 3.5 cm in height)], in order to investigate the formation of indium niobate.

Calcined powders were subsequently examined by room temperature X-ray diffraction (XRD; Siemens-D500 diffractometer), using Ni-filtered CuK_α radiation to identify the phases formed and optimum calcination conditions for the formation of $InNbO_4$ powders. Powder morphologies and particle sizes were directly imaged, using scanning electron microscopy (SEM; JEOL JSM-840A). The chemical compositions of the phase formed were elucidated by an energy-dispersive X-ray (EDX) analyzer with an ultra-thin window. EDX spectra were quantified with the virtual standard peaks supplied with the Oxford Instruments eXL software.

Results and discussion

The TG-DTA simultaneous analysis of a powder mixed in the stoichiometric proportion of $InNbO_4$ is displayed in Fig. 1. The TG curve shows two distinct weight losses. In the temperature range from room temperature to ~150 °C, both exothermic and endothermic peaks are observed in the DTA curve, in consistent with the first weight loss. These observations can be attributed to the decomposition of the organic species (i.e. polyethylene milling jar, rubber gloves, skin, etc.) from the milling process [19, 20]. Increasing the temperature up to ~1,000 °C, the solid-state reaction occurred between In_2O_3 and Nb_2O_5 [10, 16]. The broad exotherm in the DTA curve represents that reaction, which has a maximum at ~500 °C. This is supported by a large fall in sample weight over the same temperature range. The causes for these observations are not well documented, but could probably be related to (i) the partial formation of InO_6 and NbO_6 octahedra prior to $InNbO_4$ formation [6, 7] and (ii) the possible formation of $InNbO_4$ in a very small container containing only 0.5 g of powder in TG-DTA apparatus. It should be noted, however, that in the calcination process, a much larger crucible containing ~10 g of powder was used, hence, higher calcination temperature than that observed from TG-DTA is expected. Although the DTA curve shows that there are other small peaks at ~750, 850 and 900 °C, however, it is to be noted that there is no obvious interpretation of these peaks. These data were used to

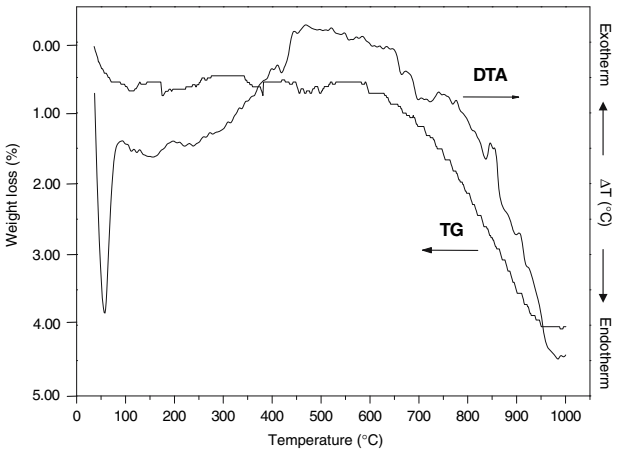

Fig. 1 TG-DTA curves for the mixture of In_2O_3–Nb_2O_5 powder

define the range of calcination temperatures for XRD investigation to between 700 °C and 1,200 °C.

To further study the phase development with increasing calcination temperature in the powders, they were calcined for 2 h in air at various temperatures, up to 1,200 °C, followed by phase analysis using XRD. As shown in Fig. 2, for the uncalcined powders and the powders calcined at 700 °C, only X-ray peaks of precursors In_2O_3 (•) and Nb_2O_5 (○), which could be matched with JCPDS file numbers 71-2195 [21] and 30-873 [22], respectively, are present, indicating that no reaction had yet been triggered during the milling or low firing processes. It is seen that fine $InNbO_4$ crystallites (∇) were developed in the powders at a calcination temperature as low as 750 °C, accompanying with In_2O_3 and Nb_2O_5 as separated phases. This observation agrees well with those derived from the TG-DTA results. As the temperature increased to 900 °C, the intensity of the wolframite-like $InNbO_4$ peaks was further enhanced and became the predominant phase. Upon calcination at 950 °C, an essentially monophasic of $InNbO_4$ phase is obtained. This $InNbO_4$ phase was indexable according to a monoclinic wolframite-type structure with lattice parameters a = 514.40 pm, b = 577.09 pm, c = 483.55 pm and β = 91.13°, space group $P2/a$ (no. 13), in consistent with JCPDS file numbers 83-1780 [23] and literature [3, 6]. This study also shows that monoclinic $InNbO_4$ is the only detectable phase in the powders, after calcination in the range of 950–1,200 °C. The variation of the intensity ratio between the two major peaks $(11\bar{1})$ and (111) at 2θ~29–31° could be attributed mainly to the expansion of the NbO_6 volume similar with those observed in other ABO_4 systems [3, 6]. In the structure of $InNbO_4$, there are two kinds of octahedron, InO_6 and NbO_6. The InO_6 octahedron connects to each other to form zigzag chain by sharing edges. These chains are connected through NbO_6 octahedron to form the three-dimensional network [6, 7, 24]. It is believed that the InO_6 chains are highly distorted because they must accommodate the strain of the defect, which probably leads to lattice rotation [11].

In earlier works [4, 6, 10, 14], long heat treatments at ~1,000–1,200 °C for 4, 12, 24 and 48 h were proposed for the formation of $InNbO_4$ by a conventional mixed oxide synthetic route, although no details on phase formation were provided. However, in the present study, it was found that, except the fluctuation of the intensity ratio between the $(11\bar{1})$ and (111) peaks, there are no significant differences between the powders calcined at 950 °C to 1,200 °C with dwell time of only 2 h, as shown in Fig. 2. This observation would clearly suggest the advantages of a rapid vibro-milling technique used in the present study.

Apart from the calcination temperature, the effect of dwell time was also found to be quite significant. From Fig. 3, it can be seen that the single phase of $InNbO_4$ (yield of 100% within the limitations of the XRD technique) was found to be possible in powders calcined at 950 °C with dwell time of 2 h or more. The appearance of In_2O_3 and Nb_2O_5 phases indicated that full crystallization has not occurred at relatively short calcination times. However, in the work reported here, it is to be noted that single phase of $InNbO_4$ powders was also successfully obtained for a calcination temperature of 900 °C with dwell time of at least 4 h

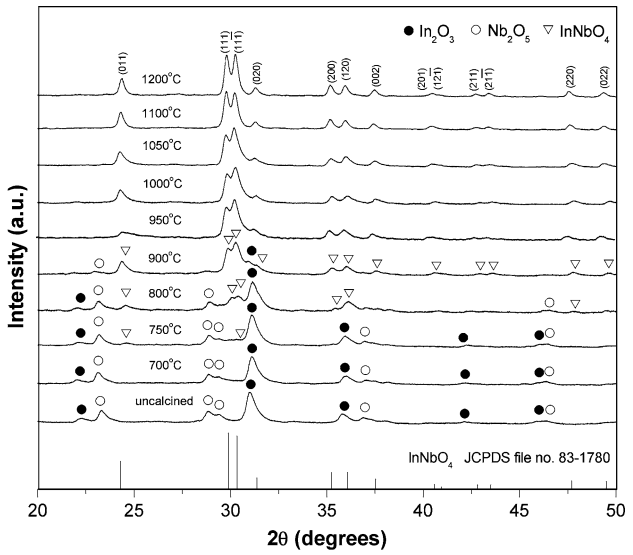

Fig. 2 XRD patterns of IN powders calcined at various temperatures for 2 h with heating/cooling rates of 10 °C/min

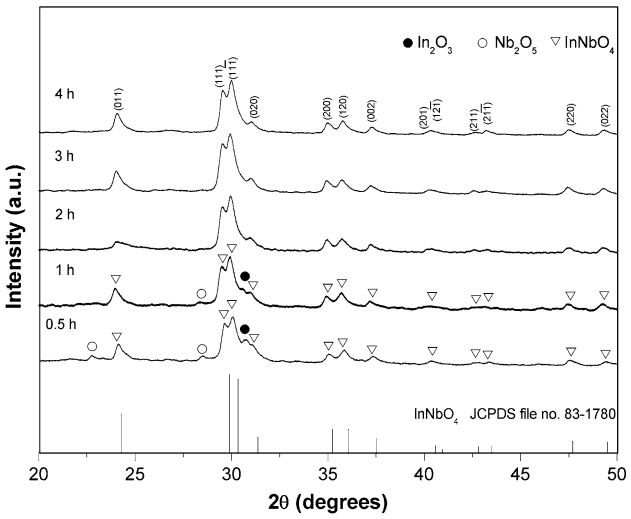

Fig. 3 XRD patterns of IN powders calcined at 950 °C with heating/cooling rates of 10 °C/min for various dwell times

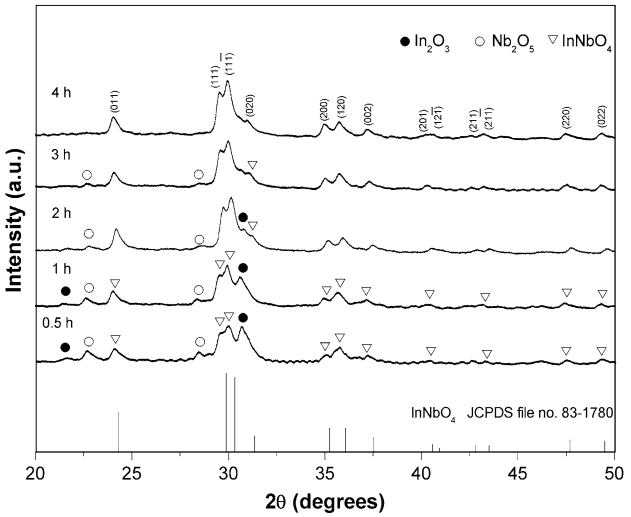

Fig. 4 XRD patterns of IN powders calcined at 900 °C with heating/cooling rates of 10 °C/min for various dwell times

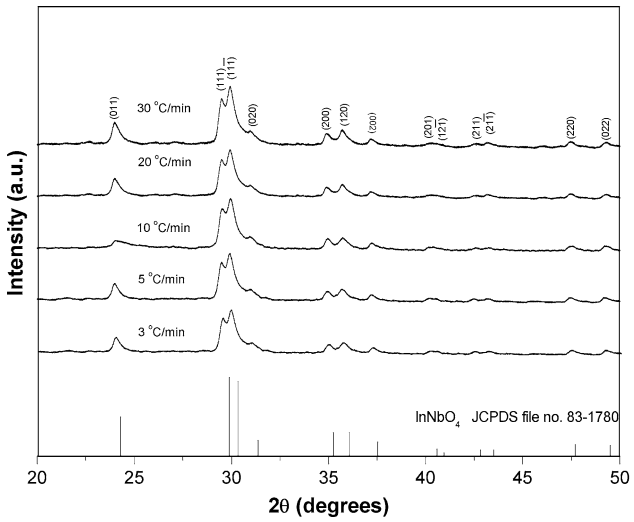

Fig. 5 XRD patterns of IN powders calcined at 950 °C for 2 h with various heating/cooling rates

applied (Fig. 4). This was apparently a consequence of the enhancement in crystallinity of the $InNbO_4$ phase with increasing dwell time. The observation that the dwell time effect may also play an important role in obtaining a single-phase wolframite product is also consistent with other similar systems [19, 25, 26]. It is also very interesting to see that the on-set firing time is approximately 2–22 h shorter than those reported earlier with a conventional ball-milling method [10–17]. The difference could be attributed to the effectiveness of vibro-milling and a carefully optimized reaction. Most importantly, this study suggests that a rapid vibro-milling method can significantly lower the optimum calcination temperature and dwell time for formation of single-phase $InNbO_4$ powders.

In the present study, an attempt was also made to calcine $InNbO_4$ powders under various heating/cooling rates. In this connection, it is shown that for the powders calcined at 950 °C for 2 h, the yield of $InNbO_4$ phase did not vary significantly with different heating/cooling rates, ranging from 3 °C/min to 30 °C/min (Fig. 5). However, for the powders calcined at 900 °C for 4 h, different result was observed. It is seen that single-phase $InNbO_4$ can be detected only in the powders where heating/cooling rates of 10 °C/min or faster were applied (Fig. 6). These results indicated that faster heating/cooling rates can probably lead to better crystallization of $InNbO_4$ phase without time for the indium vaporization (due to the volatilization of In_2O_3). The observation that faster heating/cooling rates are required for the mixtures containing *volatile* oxide constituent (In_2O_3), is in good agreement with early results reported in other similar systems [27, 28].

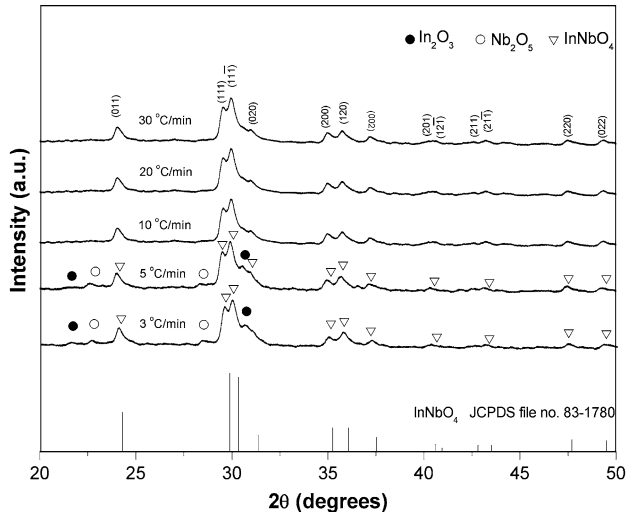

Fig. 6 XRD patterns of IN powders calcined at 900 °C for 4 h with various heating/cooling rates

Based on the TG-DTA and XRD data, it may be concluded that, over a wide range of calcination conditions, single-phase $InNbO_4$ cannot be straightforwardly formed via a solid-state mixed oxide synthetic route, unless a careful design of calcination condition is performed. It is well documented that powders prepared by a conventional mixed oxide method have spatial fluctuations in their compositions. The extent of the fluctuation depends on the characteristics of the starting powders as well as the processing schedules [20, 26]. It is rather surprising that no evidence of the monoclinic *P*2/*c* (13) of $InNbO_4$ [29, 30] was found in this study, nor was there any indication of the one with *P*2/*a* (13) reported by Brixner and Chen [3, 31] being

present. The experimental work carried out here suggests that the optimal calcination conditions for single-phase $InNbO_4$ (with impurities undetected by XRD technique) is 950 °C for 2 h or 900 °C for 4 h, with heating/cooling rates as fast as 30 °C/min. Moreover, the formation temperature and dwell time for the production of $InNbO_4$ powders observed in this work are also lower than those reported earlier [13–17]. This clearly emphasizes the advantages of a combination between a rapid vibro-milling technique and a carefully optimized reaction.

The morphological evolution during calcination was investigated by scanning electron microscopy (SEM). Micrographs of $InNbO_4$ powders calcined at various temperatures, dwell times and heating/cooling rates are illustrated in Figs. 7 and 8. The influence of calcination conditions on particle size is also given in Table 1. After calcinations at 950–1,200 °C, the powders have similar morphology (Fig. 7). In general, the particles are agglomerated and irregular in shape, with a substantial variation in particle size, particularly in samples calcined at high temperature (Fig. 7d). The results indicate that averaged particle size tends to increase with calcination temperatures and dwell times but seems to decrease with faster heating/cooling rates (Table 1). After calcinations above 950 °C (Fig. 7b–d), the powders seem to display a significant level of necking and bonding as if they were in the initial stages of sintering.

The effects of dwell time and heating/cooling rates on the morphology of the calcined powders were also found to be quite significant. As expected, it is seen that longer heat treatment leads to larger particle sizes and hard agglomeration (Figs. 7a, 8a, b). As shown in Figs. 7a, 8c, d, and also Table 1, by increasing the heating/cooling rates, averaged particle size tends to decrease whilst the degree of agglomeration tends to increase. This observation could be attributed to the mechanism of surface energy reduction of the ultrafine powders, i.e. the smaller the powder the higher the specific surface area [32]. This finding is also similar to that in $Mg_4Nb_2O_9$ powders synthesized by Ananta [33]. To the author's knowledge, the present data are the first results for the morphology–calcination relationship of $InNbO_4$ powders prepared by the solid-state reaction. It is also of interest to point out that mass production of single-phase $InNbO_4$ nanopowders with the smallest particle size ~100 nm (estimated from SEM micrographs) can be achieved by employing a simple solid-state reaction combined with a rapid vibro-milling technique. In addition, EDX analysis using a 20 nm probe on a large number of particles of the calcined powders confirms that the chemical composition is $InNbO_4$ powders, in good agreement with XRD results. For example, a chemical composition of $In_{0.95}Nb_{1.03}O_4$ can be approximated through a chemical analysis of EDX spectra in Fig. 9, which were obtained from one measurement point.

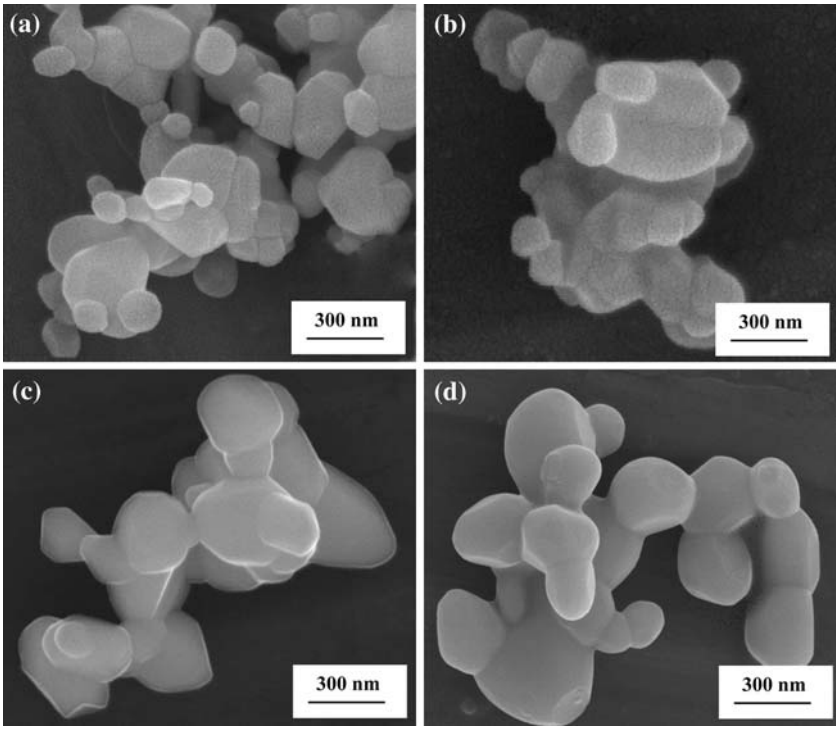

Fig. 7 SEM micrographs of the IN powders calcined for 2 h with heating/cooling rates of 10 °C/min at (**a**) 950, (**b**) 1,000, (**c**) 1,100 and (**d**) 1,200 °C

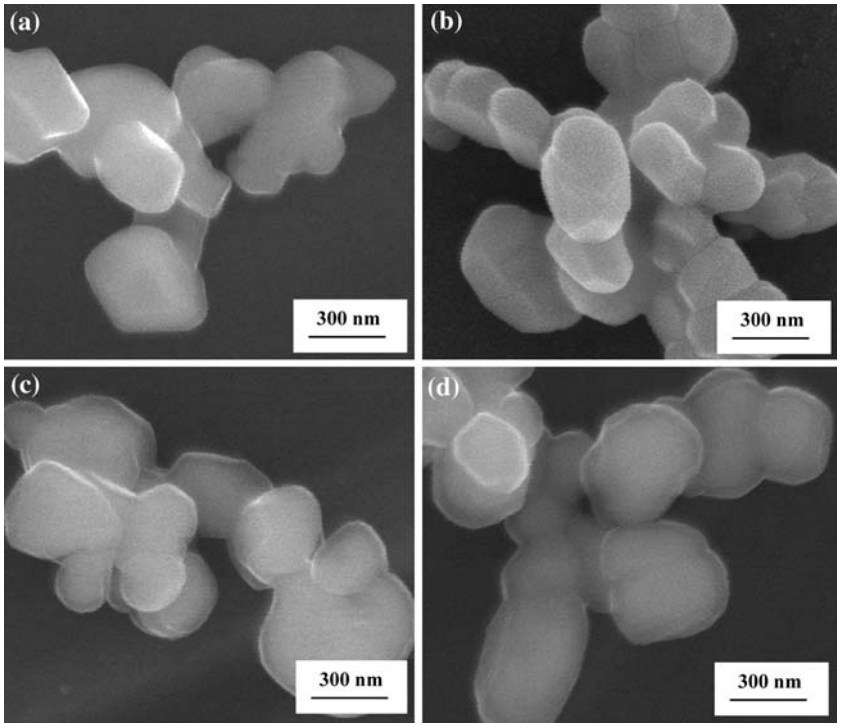

Fig. 8 SEM micrographs of the IN powders calcined at 950 °C with heating/cooling rates of 10 °C/min for (**a**) 3 h, (**b**) 4 h, and at 950 °C for 2 h with heating/cooling rates of (**c**) 3 and (**d**) 30 °C/min

Table 1 Particle size range of $InNbO_4$ powders calcined at various conditions

Calcination conditions			Estimated particle size range (±10 nm)
Temperature (°C)	Dwell time (h)	Rates (°C/min)	
900	4	10	250–600
900	4	30	200–450
950	2	3	150–550
950	2	10	150–350
950	2	30	100–350
950	3	10	300–450
950	4	10	300–700
1000	2	10	200–500
1100	2	10	250–600
1200	2	10	350–700

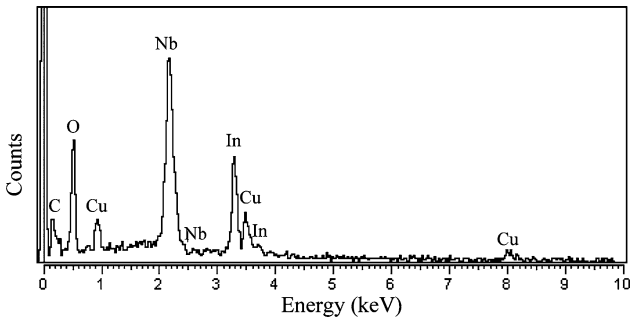

Fig. 9 EDX analysis of IN powders calcined at 950 °C for 2 h with heating/cooling rates of 30 °C/min (some spectra indexed as C and Cu come from coated electrode and sample stub, respectively)

The results obtained in this study clearly suggest that a systematic study of the effect of milling parameters such as milling times and milling speed on the phase and morphology evolutions of the $InNbO_4$ powders is required for better understanding and verifying the attractiveness of the vibro-milling technique. Further investigation of this relationship is underway and will be reported in the future.

Conclusions

The solid-state mixed oxide method via a rapid vibro-milling technique is explored in the preparation of single-phase $InNbO_4$ nanopowders. The calcination temperature, dwell time and heating/cooling rates have been found to show a pronounced effect on phase formation and particle size of the calcined $InNbO_4$ powders. This work demonstrated that single phase of indium niobate powders with particle size ranging from 100 nm to 450 nm can be produced via this technique by using a calcination temperature of 900 °C for 4 h or 950 °C for 2 h, with heating/cooling rates of 30 °C/min. The resulting $InNbO_4$ powders exhibit similar morphology and variety of agglomerated particle sizes, depending on calcination conditions.

Acknowledgements We thank the Thailand Research Fund (TRF) and the Commission on Higher Education (CHE), Graduate School and Faculty of Science, Chiang Mai University for all supports.

References

1. Keller C, Anorg Z (1962) Chem 318:89
2. Hulme JK (1953) Phys Res 92:504
3. Brixner LH, Chen H-Y (1980) Mater Res Bull 15:607
4. Zou Z, Ye J, Arakawa H (2000) Chem Phys Lett 332:271
5. Zou Z, Ye J, Sayama K, Arakawa H (2001) Nature 414:625
6. Ye J, Zou Z, Arakwa H, Oshikiri M, Shimoda M, Matsushita A, Shishido T (2002) J Photochem Photobiol A 148:79
7. Zou Z, Arakawa H (2003) J Photochem Photobiol A 158:145
8. Xu Y (1991) Ferroelectric materials and their applications. Elsevier Science, Amsterdam, The Netherlands
9. Moulson AJ, Herbert JM (2003) Electroceramics, 2nd edn. Wiley, New York
10. Alberta EF, Bhalla AS (1996) Ferroelectrics 188:95
11. Nomura K, Shingai T, Ishino S-I, Terauchi H, Yasuda N, Ohwa H (1999) J Phys Soc Jpn 68:39
12. Park SS, Choo WK (1991) Ferroelectrics 118:117
13. Alberta EF, Bhalla AS (2002) J Phys Chem Solids 63:1759
14. Elissalde C, Weill F, Ravez J (1994) Mater Sci Eng B 25:85
15. Yasuda N, Mizuno T (1995) Appl Phys Lett 66:571
16. Lee KH, Lee SB, Kim H (2004) Ceram Int 30:1035
17. Yasuda N, Inaguki H, Imamura S (1992) Jpn J Appl Phys 31:L574
18. Iwata M, Katagiri S, Orihara H, Maeda M, Suzuki I, Ohwa H, Yasuda N, Ishibashi Y (2004) Ferroelectrics 301:179
19. Ananta S, Tipakontitikul R, Tunkasiri T (2003) Mater Lett 57:2637
20. Ananta S (2004) Mater Lett 58:2834
21. Powder Diffraction File No. 71-2195 (2000) International Centre for Diffraction Data, Newton Square, PA
22. Powder Diffraction File No. 30-873 (2000) International Centre for Diffraction Data, Newton Square, PA
23. Powder Diffraction File No. 83-1780 (2000) International Centre for Diffraction Data, Newton Square, PA
24. Zou Z, Ye J, Arakawa H (2000) Chem Phys Lett 332:271
25. Youmee P, Phanichphant S, Ananta S, Heimann RB (2001) Ceram Forum Int DKG 78:E48
26. Ananta S, Brydson R, Thomas NW (1999) J Eur Ceram Soc 19:489
27. Tipakontitikul R, Ananta S (2004) Mater Lett 58:449
28. Kim BC, Lee JH, Kim JJ, Ikegami T (2002) Mater Lett 52:114
29. Powder Diffraction File No. 25-384 (2000) International Centre for Diffraction Data, Newton Square, PA
30. von Liebertz J (1972) Acta Crystallogr B 28:3100
31. Powder Diffraction File No. 33-619 (2000) International Centre for Diffraction Data, Newton Square, PA
32. Reed JS (1995) Principles of ceramics processing, 2nd edn. Wiley, New York
33. Ananta S (2004) Mater Lett 58:2530

Ferroelectrics
Publication details, including instructions for authors and subscription information:
http://www.informaworld.com/smpp/title~content=t713617887

Two-Stage Sintering of Barium Titanate Ceramic and Resulting Characteristics

To cite this Article: , 'Two-Stage Sintering of Barium Titanate Ceramic and Resulting Characteristics', Ferroelectrics, 346:1, 84 - 92
To link to this article: DOI: 10.1080/00150190601180380
URL: http://dx.doi.org/10.1080/00150190601180380

Ferroelectrics, 346:84–92, 2007

ISSN: 0015-0193 print / 1563-5112 online
DOI: 10.1080/00150190601180380

Taylor & Francis
Taylor & Francis Group

Two-Stage Sintering of Barium Titanate Ceramic and Resulting Characteristics

W. CHAISAN,* R. YIMNIRUN, AND S. ANANTA

Department of Physics, Faculty of Science, Chiang Mai University, Chiang Mai 50200, Thailand

The potential of a two-stage sintering technique as a low-cost and simple ceramic fabrication to obtain highly dense and pure barium titanate ceramics with small grain size was demonstrated in this study. Effects of designed sintering conditions on phase formation, densification, microstructure, and electrical properties of the $BaTiO_3$ ceramics were examined via X-ray diffraction (XRD), Archimedes method, scanning electron microscopy (SEM), dielectric and hysteresis measurements, respectively. It has been found that, under suitable two-stage sintering conditions, the dense perovskite BT ceramics with fine grain can be successfully achieved with good electrical properties.

Keywords Barium titanate; sintering; microstructure; dielectric properties; ferroelectric properties

1. Introduction

Barium titanate ($BaTiO_3$ or BT), which exhibits a perovskite structure and a Curie temperature $\sim$120°C, is a classical ferroelectric material that has been extensively exploited both for academic and for technological utilizations over the past decades [1, 2]. Owing to its high dielectric constant, large mechanical-quality factor, large pyroelectric coefficient, nontoxic handling and low cost of manufacturing, compared to several lead-based perovskite ferroelectrics, ceramics based on BT have been strong candidates for several electronic applications, including ultrasonic transducers, multilayer capacitors, pyroelectric detectors, semiconductors with positive temperature coefficient of resistance (PTCR) and electro-optic devices [3–7]. Because of these important technological applications, there has been a great deal of interest in the preparation process of pure BT ceramic as well as in the electrical properties of BT-based ceramics [8, 9].

Electrical properties of $BaTiO_3$ depend strongly on microstructure as well as chemical compositions [1, 6]. It was reported earlier that the high value of dielectric constant can be revealed if polycrystalline BT of fine grain size (<1 μm) is achieved [10, 11]. Thus, a fine grain is essential to achieve optimum dielectric properties. The microstructure of BT can be controlled by two approaches. Utilizing additives to prohibit the grain growth is one approach. Some additives such as Dy, Nb and Ca have been reported to be effective grain growth inhibitors [12–14]. Another approach uses novel processing technique to modify the microstructure. Numerous studies on the sintering of barium titanate have been reported

Received May 15, 2006.
*Corresponding author. E-mail: wanwilai_chaisan@yahoo.com

in the literature [11, 15, 16]. Recently, a two-stage sintering method has been proposed by Chen and Wang to achieve the densification of ceramic bodies without significant grain growth [17]. Moreover, Kim and Han [11] found that intermediate dense and fine grain size BT ceramic was achieved from the two-stage sintering technique and showed much greater dielectric constant than that of the normal sintering technique. Since the two-stage sintering process is a low-cost technique and simple ceramic fabrication to obtain highly dense ceramics with pure phase, therefore, in this work a two-stage sintering method has been adopted to produce the fine grain BT ceramic. The influence of two-stage sintering on densification, microstructure, dielectric and ferroelectric properties of the ceramics is investigated with comparison to the normal sintering scheme.

2. Experimental Procedure

$BaTiO_3$ powders used in this study were prepared by a simple mixed oxide synthetic route. Commercially available powders of $BaCO_3$ and TiO_2 (anatase form), (Fluka, >99% purity) were used as starting materials. The mixing process was carried out by ball-milling a mixture of raw materials for 24 h with corundum media in isopropyl alcohol (IPA). After wet-milling, the slurry was dried at 120°C for 2 h and calcined in a closed alumina crucible, with the optimum calcination condition determined by the XRD method (1300°C for 2 h with heating/cooling rates of 5°C/min) [18]. Ceramic fabrication was achieved by adding 1 wt% polyvinyl alcohol (PVA) binder, prior to pressing as pellets (15 mm in diameter and 1.0 to 1.3 mm thick) in a pseudo-uniaxial die press at 100 MPa. Each pellet was placed in an alumina crucible together with atmosphere powders of identical chemical composition. In the so-called two-stage sintering process, the first sintering temperature (T_1) was assigned for 1100°C and variation of the second sintering temperature (T_2) between 1200°C and 1400°C was carried out (Fig. 1). For comparison, normal sintering process was also carried out at the firing temperature between 1250 and 1450°C for 2 h with constant heating/cooling rates of 5°C/min. The two sintering schemes also included the binder burn out process at 500°C for 1 h.

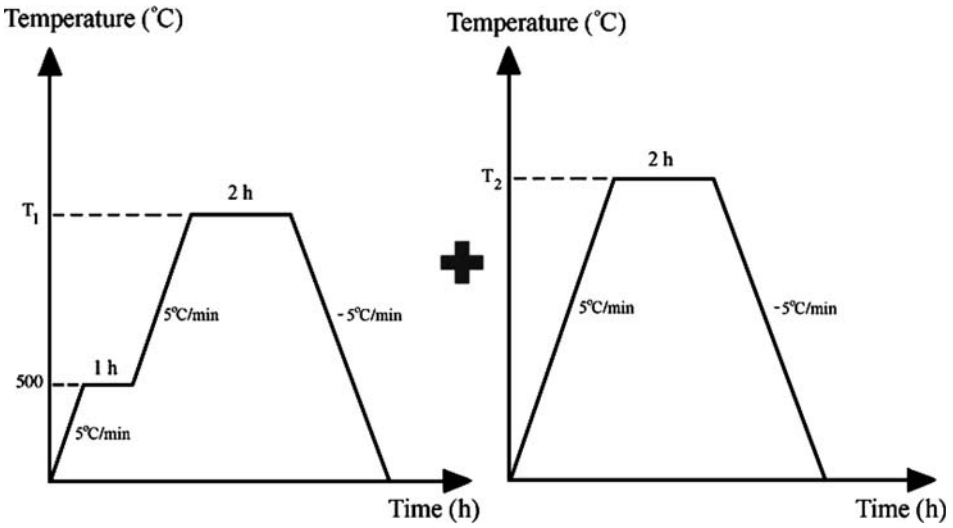

Figure 1. A two-stage method sintering profile.

Densities of the final sintered products were determined by using the Archimedes principle. Microstructural development was characterized using a JEOL JSM-840A scanning electron microscopy (SEM). Mean grain sizes of the sintered ceramics were subsequently estimated by employing the linear intercept method [19]. In order to evaluate the electrical properties, dense ceramics were polished to form flat, parallel faces (14 mm in diameter and 0.8 mm thick). Silver electrodes were then fired on both sides of the samples at 750°C for 12 min. The dielectric properties were measured at frequency of 10 kHz using a HIOKI 3532-50 LCR meter, on cooling through the transition range (200 to 25°C) with a rate of 3°C/min. For ferroelectric hysteresis characteristics, the polarization (P) was measured as a function of electric field (E), using a modified Sawyer-Tower circuit [20].

3. Results and Discussion

The XRD patterns of two stage sintered BT ceramic compared with normal sintered ceramic were illustrated in Fig. 2. The results indicated that the single phase of perovskite $BaTiO_3$ (yield of 100% within the limitations of the XRD technique) was found in both samples with no evidence of the second phase of Ba_2TiO_4, $BaTi_2O_5$ and $BaTi_3O_7$ compositions [16, 21, 22]. The strongest reflections in the majority of XRD trace indicate the formation of the perovskite phase of barium titanate ($BaTiO_3$) which could be matched with JCPDS file no. 5-0626, in agreement with other works [18, 23]. To a first approximation, this phase has a tetragonal perovskite structure in space group *P4/mm* (no. 99) with cell parameters $a =$ 399.4 pm and $c = 403.8$ pm [24]. Moreover, the XRD profiles around diffraction angles

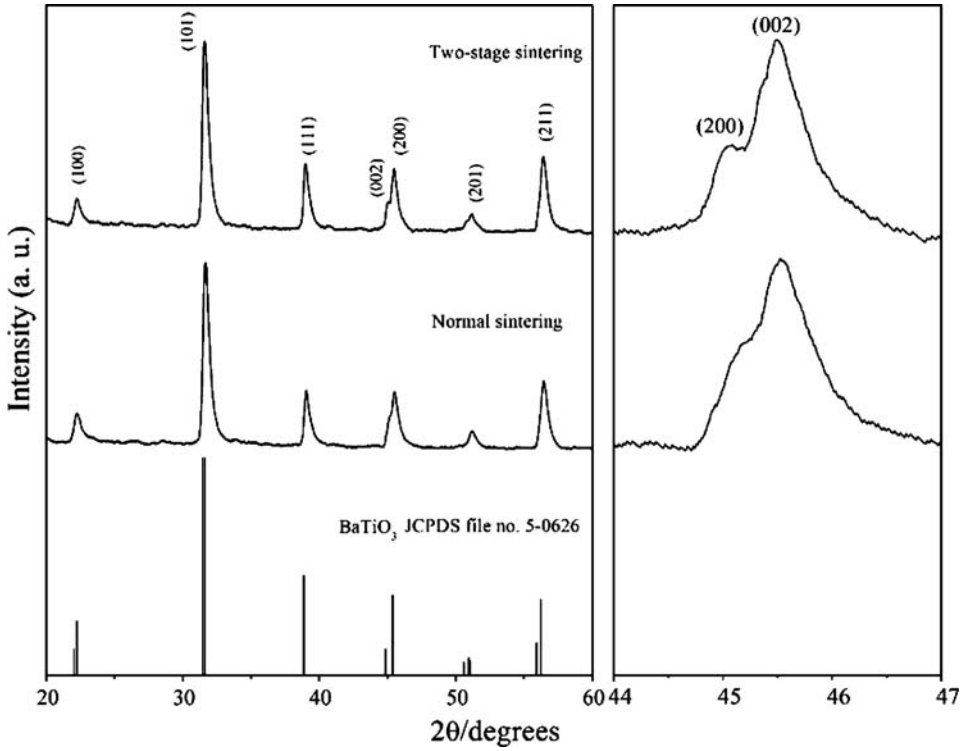

Figure 2. XRD patterns for BT ceramics.

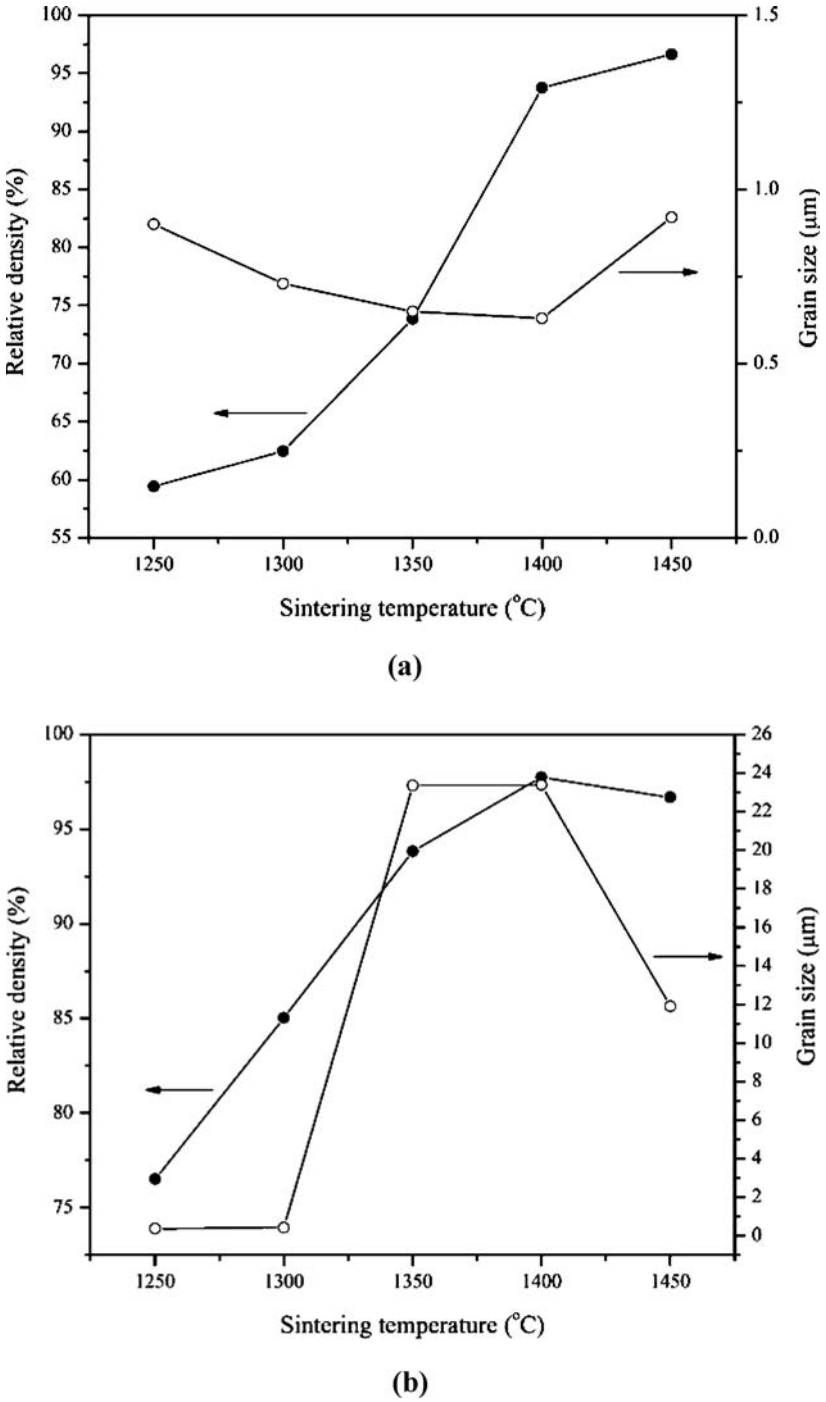

Figure 3. The relative density of sintered BT ceramics and grain size as a function of sintering temperatures: (a) two-stage sintering, with the first sintering temperature (T_1) at 1100°C and (b) normal sintering.

$2\theta \sim 44$–47° were also shown in Fig. 2. The expected positions of tetragonal (002) and (200) peaks are also indicated. The XRD data of two-stage sintered BT ceramic show a larger splitting of the tetragonal (002)/(200) peaks, as compared to the normal sintering peaks. The lattice parameters estimated from the peak position are $a = 398.3$ pm and $c = 401.6$ pm ($c/a = 1.008$), which are close to those reported previously [24].

Figure 3 shows the sintered density and average grain size of $BaTiO_3$ samples as a function of sintering temperature. In the two-stage sintering process (Figure 3a), the first sintering temperature was fixed at 1100°C, for constant dwell time of 2 h and heating/cooling rates of 5°C/min, while the second sintering temperature was varied from 1200°C to 1400°C. It can be seen that the relative density of the two-stage sintered ceramics increased significantly from 60 to 97% with increasing sintering temperature, while grain size changed only slightly (about 0.6–0.9 μm). However, in normal sintering process, while the relative density changed from 77 to 98%, similar to that of the two-stage sintering, but the average grain size increased significantly from 1 to 23 μm as the sintering temperature increased from 1250 to 1400°C. Further increase in the sintering temperature to 1450°C, the observed fall-off in density is probably due to the dominant effect of grain coarsening mechanism at high sintering temperature as suggested by other workers [25, 26]. The observation clearly signifies the advantage of the two-stage sintering technique in producing fine-grained BT ceramics.

The microstructure of BT ceramics with the highest density was revealed by SEM. Micrographs of BT samples sintered with different schemes are shown in Fig. 4. Clearly, the microstructure of the two-stage sintered ceramics (Fig. 4a) is significantly different from that of the normal sintered BT samples (Fig. 4b) which exhibit highly dense microstructure with abnormal grains of size around $\sim$50 μm due to the recrystallization during firing and variation of stoichiometric compositions [27, 28]. The two-stage sintered ceramic contains small grain size consisted with many pores. The average grain size is about 0.92 μm. Moreover, with careful observation, it can be found that BT grains in two-stage sintered ceramics also exhibit whisker-like shape. With sizes of $\sim$300–500 nm in length and $\sim$10 nm in width, these whiskers are seen to distribute and coat on the grain. Even though exact mechanism of the microstructure observed here is not well established, but it should be noted that the various features of microstructure in BT ceramics are dependent on the grain growth rate in the different planes [29]. However, the sintering process and growth environment also play an important role in the formation [30]. More importantly, it can be assumed that the two-stage sintering process could suppress the grain growth mechanism efficiently whereas the highest density of both normal- and two-stage sintered ceramics is similar in value. This can be explained that the feasibility of densification without grain growth, which is believed to occur in two-stage sintered ceramic, relies on the suppression of grain boundary migration while keeping grain boundary diffusion active. The kinetic and the driving force for grain growth behavior in the second-step sintering were previously discussed by Chen and Wang [17]. Their work suggested that the suppression of the final stage grain growth was achieved by exploiting the difference in kinetics between grain-boundary diffusion and grain-boundary migration.

The dielectric properties of sintered $BaTiO_3$, in fact, exhibit a strong dependence on grain size [10, 11, 31]. For the grain size <1 μm, anomalously high room-temperature permittivity values were obtained along with a general broadening and flattening of the permittivity peak at Curie temperature [15]. Therefore, grain size control of the sintered bodies is very important. Figure 5 shows a comparison of the dielectric properties of maximum density BT ceramics sintered by the two different schemes. It is very interesting to observe that though the average grain size of the two-stage sintered ceramic is lower than 1 μm, the Curie temperatures and the dielectric constants of the two ceramics are about the same.

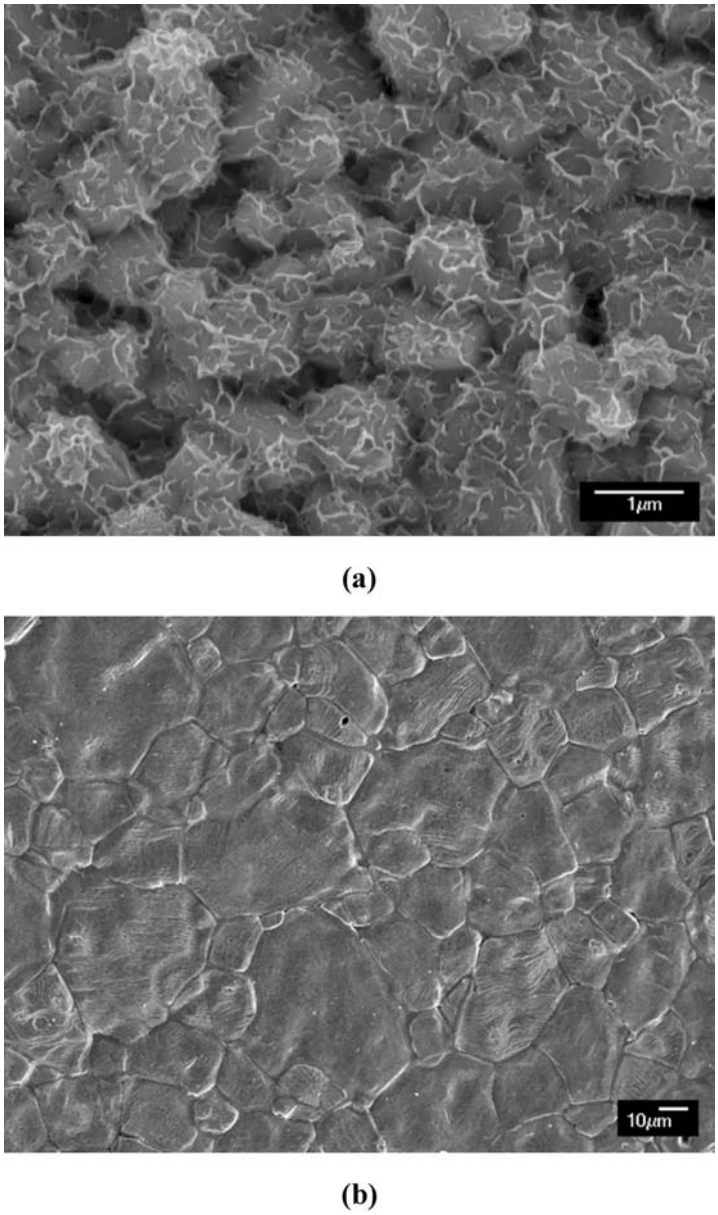

Figure 4. SEM micrographs of BT ceramics (a) two-stage sintered at 1100/1400°C, and (b) normal sintered at 1400°C.

Since the densities of the two ceramics are very similar in value (97–98%), this indicated that density could not be the controlling factor. It can be assumed that the employed sintering temperature in the two-stage sintering process is not enough for driving densification mechanism to achieve dense BT ceramics, as evidenced in Fig. 4(a). The highly porous microstructure was induced which could be the main reasons for low dielectric constant in fine grain case. However, the scope for improving two-stage sintering by raising the temperature is limited by the capability of the furnace. Nevertheless, the room temperature

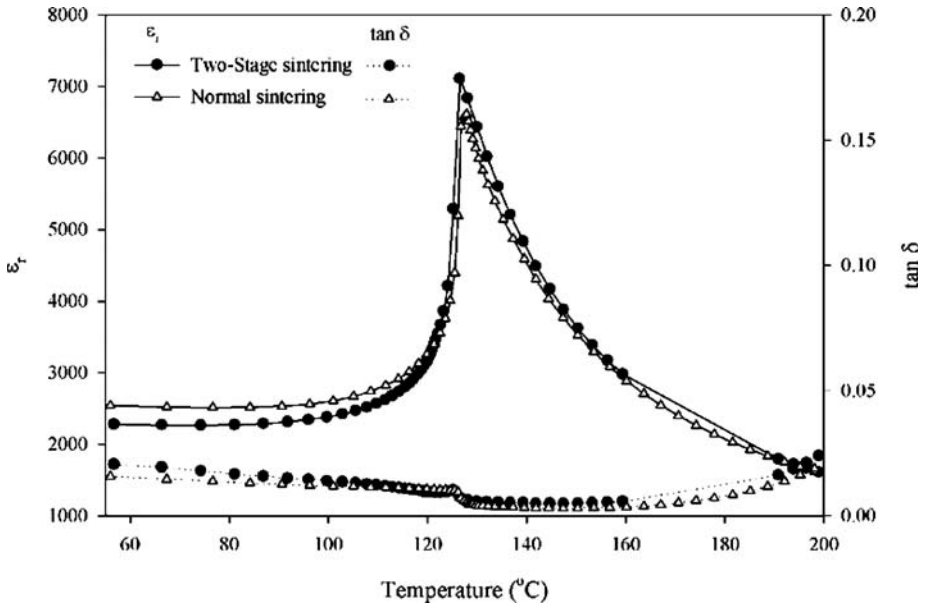

Figure 5. Variation with temperature of relative permittivity (ε_r) and dissipation factor ($\tan\delta$) at 10 kHz for two-stage sintered BT ceramics.

dielectric values in the order of 2000 for both ceramics are higher than those reported earlier [11, 23]. In the same way with the dielectric properties, the ferroelectric properties of the two-stage sintered BT ceramic were similar to those of the normal sintered ceramic, as shown in Fig. 6.

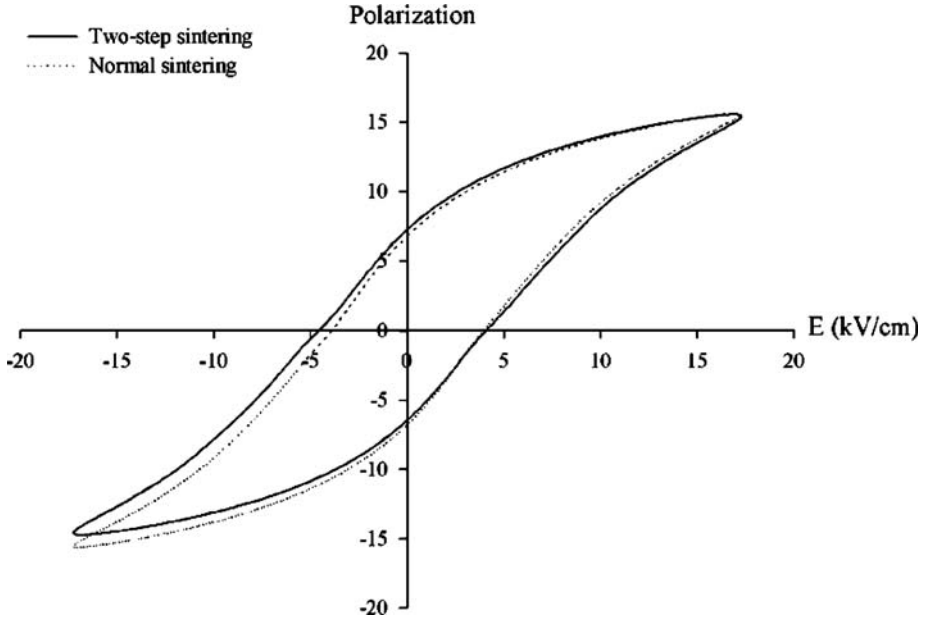

Figure 6. Hysteresis graphs of normal and two-stage sintered BT ceramics.

4. Conclusion

Even though the simple mixed-oxide method employing a conventional ball-milling was used, this work demonstrated that it was possible to obtain smaller grain size BT ceramics with high densification by the two-stage sintering technique. It has been shown that, under suitable condition, two-stage sintering can effectively suppress the grain growth in BT, leading to fine-grained microstructure ($\sim$1 μm). Moreover, whisker morphology is also found in all two-stage sintered ceramics. More importantly, the dielectric properties of BT ceramics in this work are interestingly independent of the grain size, as it is evident that dielectric constant of the small grained ceramic prepared by the two-stage sintering is of the same value with large grained ceramic prepared by the normal sintering.

Acknowledgment

We thank the Thailand Research Fund (TRF), Commission on Higher Education (CHE) the Faculty of Science, Chiang Mai University for all support.

References

1. A. J. Moulson and J. M. Herbert, Electroceramics: Materials, Properties, Applications (John Wiley & Sons Ltd., Chichester, 2003), pp. 500.
2. G. H. Haertling, *J. Am. Ceram. Soc*. **82**, 797–818 (1999).
3. K. Uchino, Piezoelectrics Actuators and Ultrasonic Motors (Kluwer, Boston, 1997), pp. 349.
4. S. L. Swartz, *IEEE Trans. Electr*. Insul. **25**, 935–987 (1990).
5. T. R. Shrout and J. P. Dougherty, *Ceramic Transactions*. **8**, 3–19 (1990).
6. Y. Xu, Ferroelectric Materials and Their Applications (Elsevier Science Publishers B. V., 1991), pp. 391.
7. K. Uchino, Ferroelectric Devices (Marcel Dekker, New York, 2000), pp. 308.
8. N. Halder, D. Chattopadhyay, A. D. Sharma, D. Saha, A. Sen, and H. S. Maiti, *Mat. Res. Bull*. **36**, 905–913 (2001).
9. B. D. Stojanovic, C. R. Foschini, M. A. Zaghete, F. O. S. Veira, K. A. Peron, M. Cilense, and J. A. Varela, *J. Mater. Process. Technol*. **113–114**, 802–806 (2003).
10. K. Kinoshita and A. Yamaji, *J. Appl. Phys*. **47**, 371–373 (1976).
11. H. T. Kim and Y. H. Han, *Ceram. Int*. **30**, 1719–1723 (2004).
12. A. Yamaji, Y. Enomoto, K. Kinoshita, and T. Murakami, *J. Am. Ceram. Soc*. **60**, 97–101 (1977).
13. M. Kahn, *J. Am. Ceram. Soc*. **54**, 452–454 (1971).
14. V. S. Tiwari, N. Singh, and D. Pandey, *J. Am. Ceram. Soc*. **77**, 1813–1818 (1994).
15. J. S. Choi and H. G. Kim, *J. Mater. Sci*. **27**, 1285–1290 (1992).
16. J. K. Lee, K. S. Hong, and J. W. Jang, *J. Am. Ceram. Soc*. **84**, 2001–2006 (2001).
17. I. W. Chen and X. H. Wang, *Nature*. **404**, 168–171 (2000).
18. W. Chaisan, S. Ananta, and T. Tunkasiri, *Cur. Appl. Phys*. **4**, 182–185 (2004).
19. R. L. Fullman, *Trans. AIME*. **197**, 447–452 (1953).
20. R. Yimnirun, S. Ananta, A. Ngamjarurojana, and S. Wongsaenmai, *Appl. Phys. A: Mat. Sci. Proc*. **81**, 1227–1231 (2005).
21. W. Maison, R. Kleeberg, R. Heimann, and S. Phanichphant, *J. Eur. Ceram. Soc*. **23**, 127–132 (2003).
22. V. Berbenni, A. Marini, and G. Bruni, *Thermochimica Acta*. **374**, 151–158 (2001).
23. W. Chaisan, R. Yimnirun, S. Ananta, and D. P. Cann, *Mater. Lett*. **59**, 3732–3737 (2005).
24. JCPDS-ICDD card no. 5-0626. International Centre for Diffraction Data, Newtown, PA, 2002.
25. F. Valdivieso, M. Pijolat, C. Magnier, and M. Soustelle, *Solid State Ionics*. **83**, 283–292 (1996).
26. G. S. Rohrer, *Annu. Rev. Mater. Res*. **35**, 99–126 (2005).

27. B. Jaffe, W. R. Cook, and H. Jaffe, Piezoelectric Ceramics (Academic Press, London, 1971), pp. 317.
28. S. H. Hur, J. K. Lee, K. W. Park, K. S. Hong, and S. J. Park, *Mater. Lett*. **35**, 78–84 (1998).
29. M. H. Lin, J. F. Chou, and H. Y. Lu, *J. Eur. Ceram. Soc*. **20**, 517–526 (2000).
30. R. M. German, Sintering Theory and Practice (Wiley, New York, 1996), pp. 550.
31. G. Arlt, D. Hennings, and G. d. With, *J. Appl. Phys*. **58**, 1619–1625 (1985).

J Mater Sci
DOI 10.1007/s10853-006-0569-7

Effects of calcination conditions on phase and morphology evolution of lead zirconate powders synthesized by solid-state reaction

W. Chaisan · O. Khamman · R. Yimnirun · S. Ananta

Received: 9 December 2005 / Accepted: 13 June 2006

Abstract Lead zirconate ($PbZrO_3$) powder has been synthesized by a solid-state reaction via a rapid vibro-milling technique. The effects of calcination temperature, dwell time and heating/cooling rates on phase formation, morphology, particle size and chemical composition of the powders have been investigated by TG-DTA, XRD, SEM and EDX techniques. The results indicated that at calcination temperature lower than 800 °C minor phases of unreacted PbO and ZrO_2 were found to form together with the perovskite $PbZrO_3$ phase. However, single-phase $PbZrO_3$ powders were successfully obtained at calcination conditions of 800 °C for 3 h or 850 °C for 1 h, with heating/cooling rates of 20 °C/min. Higher temperatures and longer dwell times clearly favored the particle growth and formation of large and hard agglomerates.

Introduction

Lead zirconate, $PbZrO_3$ (PZ), which is a typical antiferroelectric (AFE) material at room temperature with a Curie temperature of ~230 °C, has an orthorhombic symmetry with a structure similar to that of classical ferroelectric of orthorhombic barium titanate ($BaTiO_3$) [1–5]. Practically, this material is a potential candidate for energy storage applications for DC fields and low loss linear capacitor, owing to its AFE nature [6–12]. Recently, the double hysteresis behavior of this material makes it attractive for the microelectronic, microelectromechanical systems (MEMs) as well as for actuator applications [12–14].

Lead zirconate when combined with other oxides can form a series of solid solution materials such as $Pb(Zr_x,Ti_{1-x})O_3$, $PbZrO_3$–$Pb(Mg_{1/3}Nb_{2/3})O_3$, $PbZrO_3$–$PbTiO_3$–$Pb(Fe_{1/5}Nb_{1/5}Sb_{3/5})O_3$, and $PbZrO_3$–$Pb(Mg_{1/3}Nb_{2/3})O_3$, which find tremendous applications in the electroceramic industries [13–15]. In all these applications, the stoichiometry and homogeneity of materials are known to be the important factor for ensuring the performance of devices [14, 15]. This is especially important in PZT compositions in which the useful properties depend significantly on Zr/Ti ratio [1, 14, 16]. Over decades, tremendous amount of work has been dedicated to the processing of PZT with various preparation routes, one of which is a modified mixed oxide route [1, 17, 18]. In this route, the PZT is prepared by mixing precursor PZ with $PbTiO_3$ or PbO and TiO_2 powders [1, 19, 20]. This preparation route, as well as the B-site cations route, offers advantages in producing PZT with more controllable Zr/Ti ratio and desirable properties at lower sintering temperature without using excess PbO typically practiced in a more conventional mixed-oxide method [17, 21, 22]. The resulting PZT is, however, found to show variation in properties, probably caused in part by the stoichiometry of PZ precursor powders. In addition, earlier work by Reaney et al. [23] reported that impure PZ specimen showed significantly inferior electrical properties as well as unclear TEM results in the antiferroelectric–ferroelectric (AFE-FE) phase boundary as a result of unreacted ZrO_2 phases. These reasons outlined have

W. Chaisan · O. Khamman · R. Yimnirun · S. Ananta (✉)
Department of Physics, Faculty of Science, Chiang Mai University, Chiang Mai 50200, Thailand
e-mail: Supon@chiangmai.ac.th

clearly indicated from both practical and fundamental viewpoints needs to obtain stoichiometric and better homogeneity PZ. To do such, different preparative methods have been introduced, such as chemical co-precipitation [24], sol–gel [25], precipitation of molecular precursors [26], citrate combustion [27], hydrothermal [28] and microemulsion method [29]. All these techniques are aimed at reducing the temperature of preparation of the compound even though they are more involved and complicated in approach than the solid-state reaction method. Moreover, high purity PZ powders are still not available in mass quantity and also expensive. So far, only limited attempts have been made to improve the yield of $PbZrO_3$ by optimizing calcination conditions [30–32]. The effects of applied dwell time and heating/cooling rates have not yet been studied extensively. Therefore, it is our interest to explore a simple mixed oxide synthetic route for the production of PZ powders. The effect of calcination conditions on the development of phase, morphology and particle size of lead zirconate powders is investigated in this connection. The potential of a vibro-milling technique as a significant time-saving method to obtain single-phase lead zirconate powders, at low temperature and with small particles is also examined.

Experimental procedure

The starting materials were commercially available lead oxide, PbO (JCPDS file number 77-1971) and zirconium oxide, ZrO_2 (JCPDS file number 37-1484) (Fluka, >99% purity). The two oxide powders exhibited an average particle size in the range of 3.0–5.0 μm. $PbZrO_3$ powders were synthesized by the solid-state reaction of thoroughly ground mixtures of PbO and ZrO_2 powders that were milled in the required stoichiometric ratio. Instead of employing a ball-milling procedure (ZrO_2 media under ethanol for 24 h [30] or under a mixture of cyclohexane and deionized water for 12 h [31]), use was made of a McCrone vibro-milling technique [22, 32, 33]. In order to combine mixing capacity with a significant time saving, the milling operation was carried out for 0.5 h with corundum cylindrical media in isopropyl alcohol (instead of 8 h with zirconia media [32]). After drying at 120 °C for 2 h, the reaction of the uncalcined powders taking place during heat treatment was investigated by themogravimetric and differential thermal analysis (TG-DTA, Shimadzu), using a heating rate of 10°C/min in air from room temperature up to 1000 °C. Based on the TG-DTA results, the mixture was calcined at various conditions, i.e. temperatures ranging from 700 to 900 °C, dwell times ranging from 1 to 5 h and heating/cooling rates ranging from 1 to 20 °C/min, in closed alumina crucible, in order to investigate the formation of lead zirconate.

Calcined powders were subsequently examined by room temperature X-ray diffraction (XRD; Siemens-D500 diffractometer), using Ni-filtered CuK_α radiation to identify the phases formed and optimum calcination conditions for the formation of $PbZrO_3$ powders. Crystallite sizes and lattice parameters in the calcined powders were estimated from XRD data [34, 35]. Powder morphologies and particle sizes were directly imaged, using scanning electron microscopy (SEM; JEOL JSM-840A).

Results and discussion

The TG-DTA simultaneous analysis of a powder mixed in the stoichiometric proportions of $PbZrO_3$ is displayed in Fig. 1. In the temperature range from room temperature to ~150 °C, the sample shows both exothermic and endothermic peaks in the DTA curve, in consistent with a slight drop in weight loss at the same temperature range. These observations can be attributed to the decomposition of the organic species (most likely polyethylene from the milling jar) from the milling process. [22, 33]. Corresponding to a large fall in sample weight (~4.5%), the other exotherm and endotherm are observed within 300–450 °C temperature range in the DTA curve. However, it is to be noted that there is no obvious interpretation of these peaks, although it is likely to correspond to a phase transformation of ZrO_2 precursor alloyed with PbO precursor reported by a number of workers [35–38]. In general, it is well established that there are a number of polymorphic forms of PbO and ZrO_2 stable at different temperatures and pressures [35, 37]. However, in this

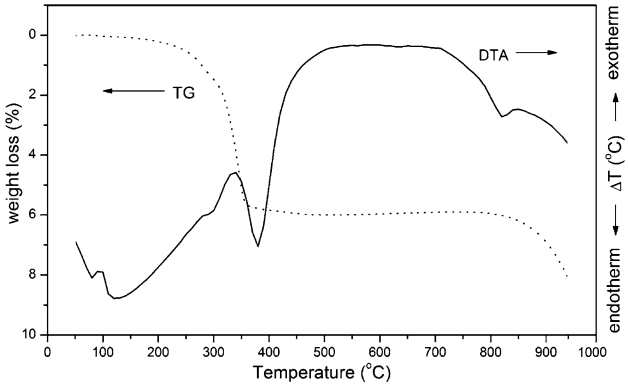

Fig. 1 TG-DTA curves for the mixture of PbO–ZrO_2 powders

work, the possibility of these phase transformations has not been investigated, since the overriding objective is to synthesize single phase $PbZrO_3$, irrespective of the polymorph in which it is stabilized.

Increasing the temperature up to ~1000 °C, the solid-state reaction occurred between PbO and ZrO_2 [29–32]. The broad exotherm from 500 to 700 °C in the DTA curve represents that reaction, which is supported by a gradual decrease in sample weight over the same temperature range. Finally, a significantly drop in weight loss is also observed above 800 °C, that is associated with the DTA peaks at the same temperature range and may be attributed to the PbO volatilization commonly found in the lead-based perovskite systems [22, 33, 39]. These data were used together with those from literature [30–32] to assign the range of calcination temperatures for XRD investigation between 700 and 900 °C.

Therefore, to investigate the effect of calcination temperature on the phase development, the mixed powders were calcined for 2 h in air at various temperatures, up to 900 °C, followed by phase analysis using XRD. As shown in Fig. 2, for the uncalcined powder, only X-ray peaks of precursors PbO (▼) and ZrO_2 (●), which could be matched with JCPDS file numbers 77-1971 [40] and 37-1484 [41], respectively, are present, indicating that no reaction had yet been triggered during the milling process. It is seen that fine $PbZrO_3$ crystallites (*) were developed in the powder at a calcination temperature as low as 750°C, accompanying with PbO and ZrO_2 as separated phases. This observation agrees well with those derived from the TG-DTA results and other workers [31, 38]. As the temperature increased to 800 °C, the intensity of the perovskite-like $PbZrO_3$ peaks was further enhanced and became the predominant phase. Upon calcination at 850 °C, an essentially monophasic of $PbZrO_3$ phase is obtained. This PZ phase was indexable according to an orthorhombic perovskite-type structure with lattice parameters a = 823.1 pm, b = 1177 pm and c = 588.1 pm, space group *P2cb* (no. 32), in consistent with JCPDS file numbers 35-739 [42] and other investigators [24, 30, 43]. This study also shows that crystalline orthorhombic PZ is the only detectable phase in the powder, after calcination in the range 850–900 °C.

Having established the optimum calcination temperature, dwell times ranging from 1 to 5 h with constant heating/cooling rates of 5°C/min were applied at 850 and 800 °C, as shown in Figs. 3 and 4, respectively. From Fig. 3, it can be seen that the single phase of $PbZrO_3$ (yield of 100% within the limitations of the XRD technique) was found to be possible in all powders calcined at 850 °C with dwell time ranging from 1 to 5 h. This is probably due to the effectiveness of vibro-milling and a carefully optimized reaction. However, in the work reported here, it is to be noted that single-phase of $PbZrO_3$ powders was also successfully obtained for a calcination temperature of 800 °C with dwell time of 3 h or more applied (Fig. 4). This was apparently a consequence of the enhancement in crystallinity of the $PbZrO_3$ phase with increasing dwell time. The appearance of PbO phase indicated that full crystallization has not occurred at relatively shorter calcination times. The observation

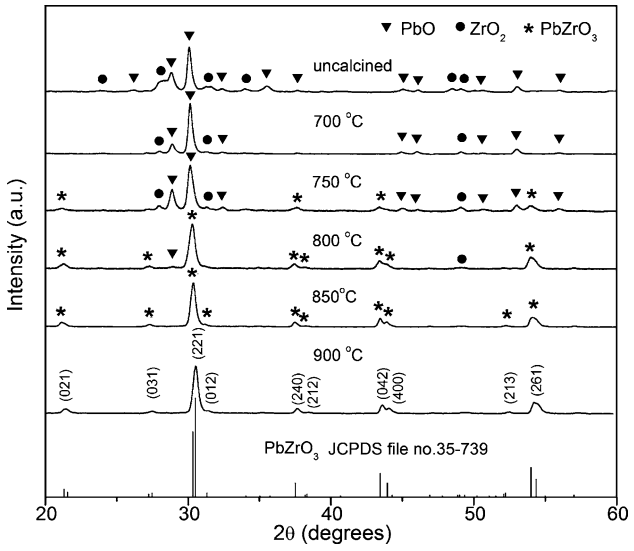

Fig. 2 XRD patterns of PZ powder calcined at various temperatures for 1 h with heating/cooling rates of 10°C/min

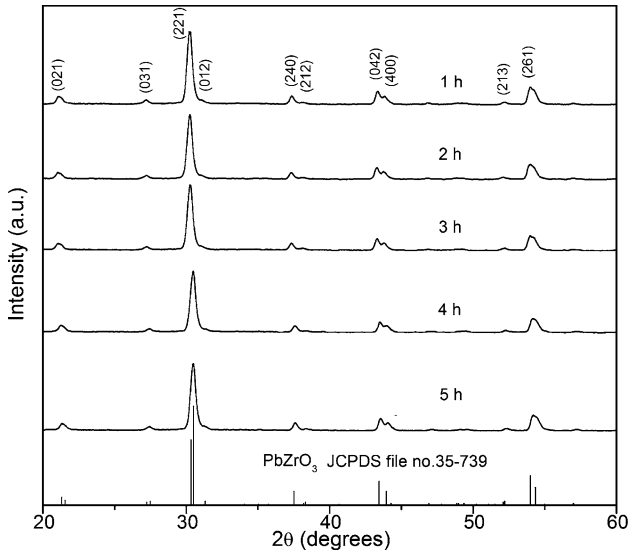

Fig. 3 XRD patterns of PZ powder calcined at 850 °C with heating/cooling ratesof 10 °C/min for various dwell times

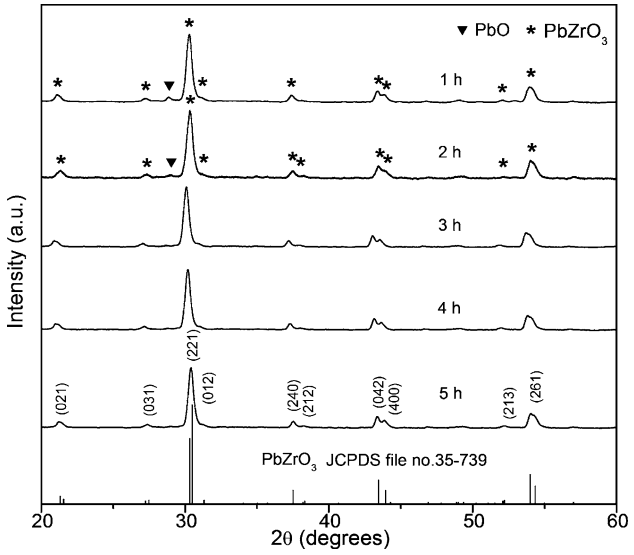

Fig. 4 XRD patterns of PZ powder calcined at 800 °C with heating/cooling rates of 10 °C/min for various dwell times

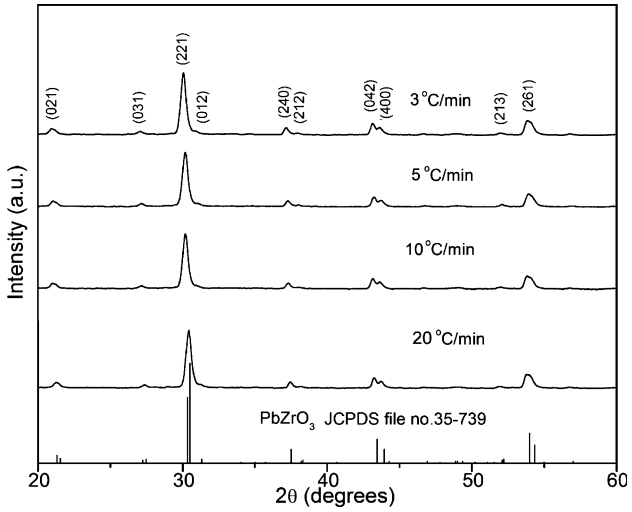

Fig. 6 XRD patterns of PZ powder calcined at 850 °C for 1 h with various heating/cooling rates

that the dwell time effect may also play an important role in obtaining a single-phase perovskite product is also consistent with other similar systems [33, 39, 44].

Apart from the calcination temperature and dwell time, the effect of heating/cooling rates on the formation behavior of $PbZrO_3$ was also investigated. Various heating/cooling rates ranging from 1 to 20 °C/min were selected for calcination conditions of 800 °C for 3 h (Fig. 5) and 850 °C for 1 h (Fig. 6). In this connection, it is shown that the yield of $PbZrO_3$ phase was not depending on heating/cooling rates, indicating that fast heating/cooling rates can lead to full crystallization of $PbZrO_3$ phase without time for the formation of minor

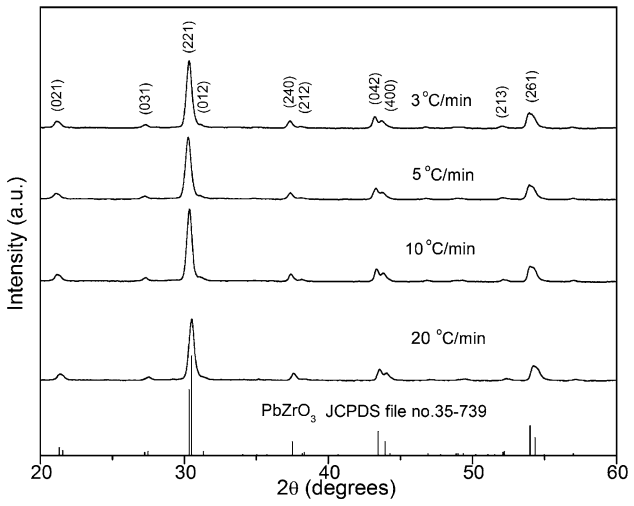

Fig. 5 XRD patterns of PZ powder calcined at 800 °C for 3 h with various heating/cooling rates

phase or lead vaporization. The observation that faster heating/cooling rates are required for lead-based ferroelectrics is also consistent with other researchers [39, 45, 46]. It should be once again emphasized that these results clearly indicate effects of heating/cooling rates on the phase formation behavior of PZ powders. These parameters are very crucial for Pb-based compounds [22, 47]. Usually, heating/cooling rates and dwell time show marked influences on phase formation behavior of other Pb-based compounds, such as PZT. It is of interest to observe that in PZ powders the heating/cooling rates do not show any effects on the behavior, while the dwell time only shows the effects on the particle agglomeration.

Based on the TG-DTA and XRD data, it may be concluded that, over a wide range of calcination conditions, single phase $PbZrO_3$ cannot be straightforwardly formed via a solid-state mixed oxide synthetic route, unless carefully designed calcination condition was performed. It is well documented that powders prepared by a conventional mixed oxide method have spatial fluctuations in their compositions. The extent of the fluctuation depends on the characteristics of the starting powders as well as the processing schedules [22, 33, 39]. The experimental work carried out here suggests that the optimal calcination conditions for single-phase $PbZrO_3$ (with impurities undetected by XRD technique) is 800 °C for 3 h or 850 °C for 1 h, with heating/cooling rates of 20 °C/min, which is closed to that of Puchmark et al. [30] (775 °C for 3 h with heating/cooling rates of 5 °C/min) but with significantly faster heating/cooling rates. Moreover, the formation temperature and/or dwell time for the production of

$PbZrO_3$ powders observed in this work are also lower than those reported by Fang et al. [31] (900 °C for 1 h) and Lanagan et al. [32] (900 °C for 8 h).

Finally, the morphological changes in the $PbZrO_3$ powders formed by a mixed oxide are illustrated in Fig. 7 as a function of calcination temperatures, dwell times and heating/cooling rates, respectively. The influence of calcination conditions on particle size is given in Table 1. These particle size data were directly estimated from SEM micrographs. Even though these data are not precisely determined, they were shown to provide estimated comparison between different calcination conditions and to form a basis for other more detailed studies with use of a combination between TEM and particle size distribution analyzer. After calcinations at 800 to 900°C, the powders seem to have similar morphology. In general, the particles are agglomerated and irregular in shape, with a substantial variation in particle size, particularly in samples calcined at higher temperatures or for longer dwell times. This observation is also similar to that of $Mg_4Nb_2O_9$ powders synthesized by Ananta [48]. The results indicate that averaged particle size and degree of agglomeration tend to increase with calcination temperature and dwell time (Table 1). However, the smallest particle size (estimated from SEM micrographs to be ~250 nm) and the morphology of the calcined powders are about the same. It is also of interest to point out that no evidence has been obtained for the existence of the cubic or spherical shape morphology as that of the hydrothermally derived $PbZrO_3$ powders [28, 49].

Conclusions

The methodology presented in this work provides a simple method for preparing perovskite $PbZrO_3$ powders via a solid-state mixed oxide synthetic route. By using optimal calcination conditions of 800 °C for 3 h or 850 °C for 1 h, with heating/cooling rates of 20 °C/min, the reproducible, low cost and fast process involving vibro-milling can provide high-purity perovskite $PbZrO_3$ powders with particle size ranging from 200–500 nm from inexpensive commercially available raw materials. The resulting $PbZrO_3$ powders consist of variety of agglomerated particle sizes, depending on calcination conditions. Finally, it should be emphasized that this work presents for the first time the effects of calcination conditions on the phase formation behavior of the PZ powders. These parameters clearly show significant influences on the processing of even simple binary system as PZ, and there is no doubt that they will show even more effects on other complicated materials such as PZT, PMN, PZN, PIN, and PMN-PT. The results on those systems are being produced and will be presented in future publications.

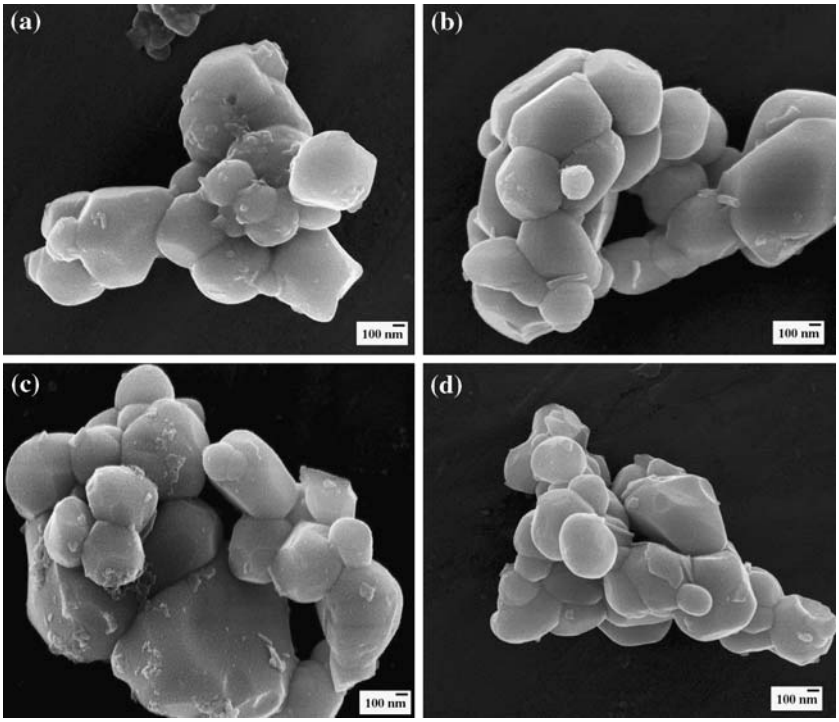

Fig. 7 SEM micrographs of the PZ powders calcined at (**a**) 850 °C/1h, (**b**) 850 °C/2 h, (**c**) 900 °C/2 h, with heating/cooling rates of 10 °C/min and (**d**) 850 °C/1 h with heating/cooling rates of 20 °C/min

Table 1 Particle size range of $PbZrO_3$ powders calcined at various conditions

Temperature (°C)	Dwell time(h)	Heating/cooling rates(°C/min)	Particle size range (mean)*(μm)
800	3	3	0.35–0.60 (0.41)
800	3	5	0.15–1.00 (0.52)
850	1	3	0.30–1.00 (0.44)
850	1	5	0.30–0.80 (0.59)
850	1	10	0.25–0.70 (0.54)
850	1	20	0.30–0.80 (0.51)
850	2	10	0.25–1.20 (0.64)
900	2	10	0.35–1.50 (0.77)

*The estimated precision of the particle size is ±10%

Acknowledgements We thank the Thailand Research Fund (TRF), the Comission on Higher Education (CHE), Graduate School, Faculty of Science, and Center of Excellence in Functional Nanomaterials, Chiang Mai University for all supports.

References

1. Jaffe B, Cook WJ, Jaffe H (1971) Piezoelectric ceramics. Academic Press, London
2. Jona F, Shirane G (1993) Ferroelectric crystals. Dover Publications, New York
3. Sawaguchi E, Maniwa H,Hoshino S (1951) Phys Rev 83:1078
4. Shirane G, Sawaguchi E, Takagi Y (1951) Phys Rev 84:476
5. Sawaguchi E, Kittaka K (1952) J Phys Soc Jpn 7:336
6. Tennery VJ (1966) J Am Ceram Soc 49:483
7. Scott BA, Burns G (1972) J Am Ceram Soc 55:331
8. Shirane G, Hoshino S (1954) Acta Crystallogr **7**:203
9. Pokharel BP, Pandey D (1999) J Appl Phys 86:3327
10. Bongarn T, Rujijanagul G, Milne SJ (2005) Mater Lett 59:1200
11. Whatmore RW (1976) Ph.D. Thesis, Genville and Cauis College, Cambridge
12. Singh K (1989) Ferroelectrics 94:433
13. Haertling GH (1999) J Am Ceram Soc 82:797
14. Moulson AJ, Herbert JM (2003) Electroceramics, 2nd edn. Wiley, New York
15. Uchino K (1998) Piezoelectrics and ultrasonic applications. Kluwer, Deventer
16. Kakegawa K, Mohri J, Takahashi T, Yamamura H, Shirasaki S (1977) Solid State Commun 24:769
17. Kingon AI, Clark JB (1983) J Am Ceram Soc 66:253
18. Matsuo Y, Sasaki H (1965) J Am Ceram Soc 48:289
19. Babushkin O, Lindback T, Lue JC, Leblais JYM (1996) J Eur Ceram Soc 16:1293
20. Hanky DL, Biggers JV (1951) J Am Ceram Soc 12:172
21. Garg A, Agrawal DC (1999) Mat Sci Eng B 56:46
22. Tipakontitikul R, Ananta S (2004) Mater Lett 58:449
23. Reaney IM, Glazounov A, Chu F, Bell A, Setter N (1997) Brit Ceram Trans 96:217
24. Oren EE, Taspinar E, Tas AC (1997) J Am Ceram Soc 80:2714
25. Ibrahim DM, Hennicke HW (1981) Trans J Br Ceram Soc 80:18
26. Deshpande AS, Khollam YB, Patil AJ, Deshpande SB, Potdar HS, Date SK (2001) Mater Lett 51:161
27. Rao YS, Sunandana CS (1992) J Mater Sci Lett 11:595
28. Choi JY, Kim CH, Kim DK (1998) J Am Ceram Soc 81:1353
29. Fang J, Wang J, Ng SC, Gan LM, Quek CH, Chew CH (1998) Mater Lett 36:179
30. Puchmark C, Rujijanagul G, Jiansirisomboon S, Tunkasiri T (2004) Ferroelectric Lett 31:1
31. Fang J, Wang J, Ng SC, Gan LM, Chew CH (1998) Ceram Inter 24:507
32. Lanagan MT, Kim JH, Jang S, Newnham RE (1988) J Am Ceram Soc 71:311
33. Ananta S, Thomas NW (1999) J Eur Ceram Soc 19:155
34. Klug H, Alexander LE (1974) X-ray diffraction procedures for polycrystalline and amorphous materials, 2nd edn. Wiley, New York
35. Aoyama T, Kurata N, Hirota K, Yamaguchi O (1995) J Am Ceram Soc 78:3163
36. Fushimi S, Ikeda T (1967) J Am Ceram Soc 50:129
37. Lee WE, Rainforth WM (1994) Ceramic microstructures: Property control by processing. Chapman & Hall, London
38. Deyneka TG, Vouk EA, Ishchuk VM, Ramakaeva RF, Volkova GK, Konstantinova TE (2004) Funct Mater 11:44
39. Udomporn A, Ananta S (2004) Mater Lett 58:1154
40. JCPDS-ICDD Card No. 77-1971 (2002) International Centre for Diffraction Data, Newtown Square, PA
41. JCPDS-ICDD Card No. 37-1484 (2002) International Centre for Diffraction Data, Newtown Square, PA
42. JCPDS-ICDD Card No. 35-739 (2002) International Centre for Diffraction Data, Newtown Square, PA, 2002
43. Tani T, Li JF, Viehland D, Payne DA (1994) J Appl Phys 75:3017
44. Ananta S, Brydson R, Thomas NW (2000) J Eur Ceram Soc 20:2315
45. Ryu J, Choi JJ, Kim HE (2001) J Am Ceram Soc 84:902
46. Baumgartner CE (1988) J Am Ceram Soc 71:C-350
47. Udomporn A, Pengpat K, Ananta S (2004) J Eur Ceram Soc 24:185
48. Ananta S (2004) Mater Lett 58:2530
49. Kim HK (1993) Thesis MS, Seoul National University, Seoul, Korea

Appl. Phys. A (2007)
DOI: 10.1007/s00339-007-3932-x

Applied Physics A
Materials Science & Processing

R. YIMNIRUN[1,✉]
X. TAN[2]
S. ANANTA[1]
S. WONGSAENMAI[1]

Preparation of fine-grain lead indium niobate ceramics with wolframite precursor method and resulting electrical properties

[1] Department of Physics, Faculty of Science, Chiang Mai University, Chiang Mai 50200, Thailand
[2] Department of Materials Science and Engineering, Iowa State University, Ames, IA 50011, USA

Received: 5 October 2006/Accepted: 30 January 2007

ABSTRACT In this study, lead indium niobate ($Pb(In_{1/2}Nb_{1/2})O_3$ or PIN) ceramics were prepared by a wolframite precursor method via a vibro-milling technique. Fine-grain ceramics were achieved with average grain size of 1–2 μm, indicating advantage of the vibro-milling technique used. The dielectric and ferroelectric properties were measured by means of an automated dielectric measurement set-up and a standardized ferroelectric tester, respectively. The dielectric properties of PIN ceramic were measured as functions of both temperature and frequency. The results indicated that the dielectric properties of the PIN ceramic were of relaxor ferroelectric behavior with temperature of dielectric maximum (T_m) ∼ 53 °C and dielectric constant (ε_r) ∼ 4300 (at 1 kHz). The P–E hysteresis loop measurements at various temperatures showed that the ferroelectric properties of the PIN ceramic changed from the paraelectric behavior at temperature above T_m to slim-loop type relaxor behavior at temperature slightly below T_m. Moreover, the P–E loop became more open at temperatures much lower than T_m.

PACS 77.22.Ch; 77.84.Dy

1 Introduction

Lead indium niobate $Pb(In_{1/2}Nb_{1/2})O_3$ (PIN) compounds are of interest for the kinetics of compositional ordering investigation [1]. It has been reported that the degrees of ordering on the B-site can be varied by thermal annealing and by forming solid solutions with perovskite compounds that exhibit normal dielectric behavior, such as $Pb(Fe_{1/2}Nb_{1/2})O_3$ (PFN), $PbZrO_3$ (PZ) and $PbTiO_3$ (PT) [2]. With different thermal treatments, the degrees of the In/Nb cation ordering on the B-site in a perovskite structure can be manipulated from a structurally disordered state into various degrees of ordering. The disorder PIN is a relaxor ferroelectric with a pseudo-cubic perovskite structure exhibiting the relaxor behavior with a broad dielectric maximum near 66 °C, when measured at 1 kHz [3, 4]. On the other hand, the ordered PIN has the antiferroelectric orthorhombic phase [5–9] with a sharp peak in the dielectric constant at 168 °C [4, 10]. However, phase-pure perovskite PIN ceramics free of the pyrochlore phase are very difficult to prepare using a conventional mixed oxide method [7, 11]. This is because the tolerance and the electronegativity difference of PIN are very low compared with other perovskite compounds such as PMN [2, 12]. The wolframite method, as used by Groves [13] for the preparation of perovskite PIN ceramic, is not effective in suppressing pyrochlore phase formation. The addition of excess In_2O_3 was shown to yield higher amount of perovskite phase (up to 98%) [13]. Recently, Alberta and Bhalla [7] were able to produce 100% phase-pure perovskite PIN ceramic with the addition of excess indium and/or lithium with wolframite method under oxygen atmosphere. Interestingly, these previous studied employed a mixed-oxide method with a conventional ball-milling technique. The powders prepared by the conventional mixed oxide route usually have spatial fluctuations in their compositions, which may lead to formation of unwanted phases. The extent of the fluctuation depends on the characteristics of the starting powders as well as on the processing schedule. Many recent studies have paid attention to processing schedule in details to yield phase-pure powders in many perovskite systems [14–20]. In addition, a vibro-milling technique has recently been employed to produce nano-sized powders which can also be used to fabricate ceramics with fine-grain microstructure that may lead to better resulting properties [14, 16, 20]. Therefore, the main purpose of this work is to prepare PIN powders and ceramics with the wolframite method via the vibro-milling technique. The vibro-milling technique is employed in this study to explore the potential in obtaining fine-grain ceramics, which would in turn lead to superior electrical properties. The effects of processing conditions on the phase formation behavior are also investigated. More importantly, the dielectric and ferroelectric properties of the resulting ceramics are also studied.

2 Experimental

The $Pb(In_{1/2}Nb_{1/2})O_3$ ceramics were prepared from $Pb(In_{1/2}Nb_{1/2})O_3$ powders obtained with the wolframite method via the vibro-milling technique. In this technique, a vibratory laboratory mill (McCrone micronizing mill) was employed. A total of 48 polycrystalline corundum milling media with a powder weight of 20 g was kept constant in each batch. The milling operation was carried out in isopropanal inert to the polypropylene jar [14, 16, 20]. Initially,

✉ Fax: +6653-943-445, E-mail: rattikornyimnirun@yahoo.com